

Master in Electrical and Electronics Engineering

EE-517: Bio-Nano-Chip Design

Lecture #7 Checking Probes-layer quality (RM+SPR+SEM+AFM)

Lecture Outline

(Book Bio/CMOS: Chapter' paragraphs §5.2.1-2)

- Resonant Mirror
- Surface Plasmon Resonance
- Scanning Electron Microscopy
- Atomic Force Microscopy
- Scanning Tunneling Microscopy

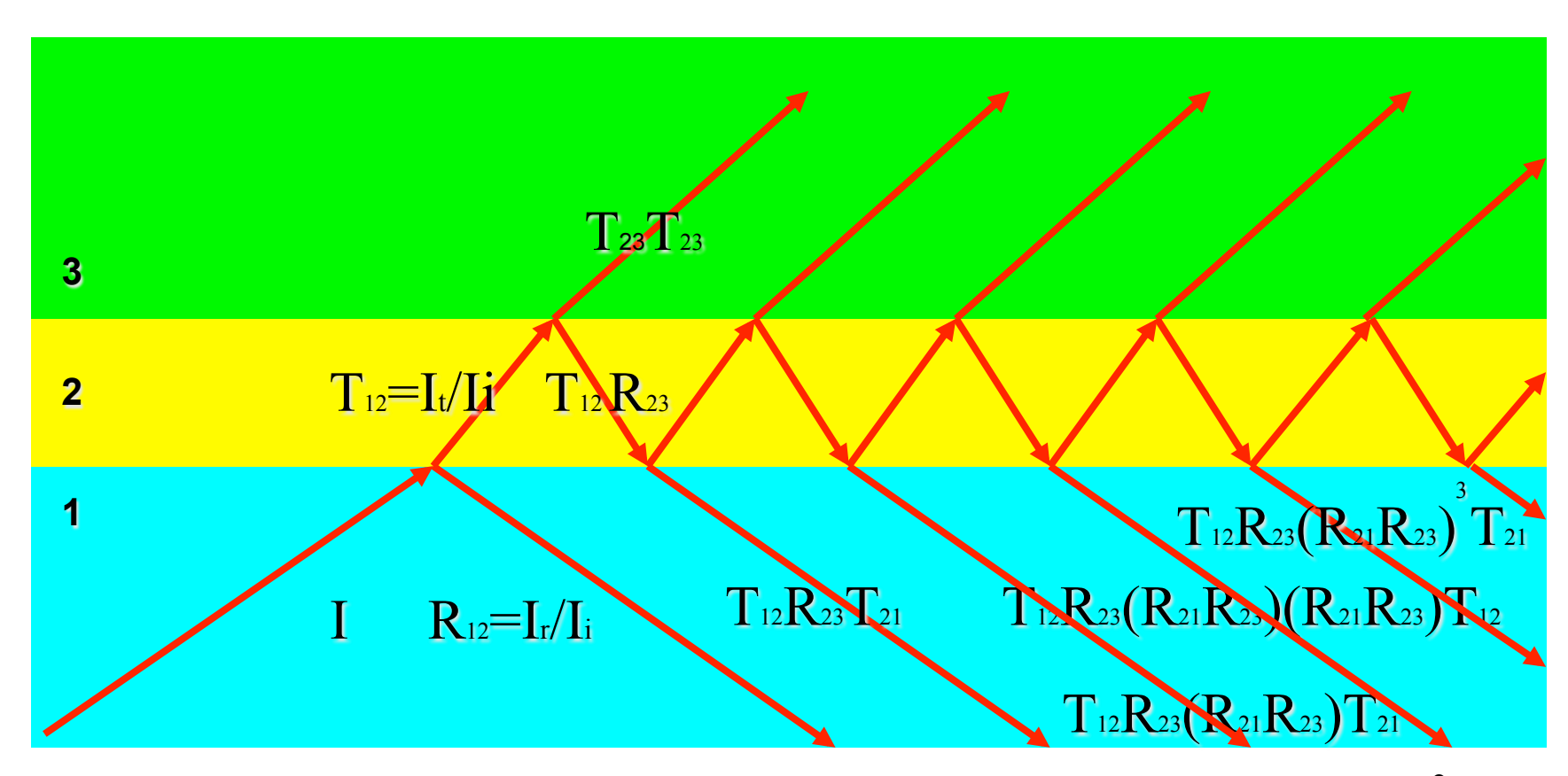
How to characterize the Probes Immobilization?

We have seen what are the mechanisms of self-assembly!

How to monitor the self-assembly process?

How to check the film quality?

Three-layers Reflection



$$R = R_{12} + T_{12}R_{23}T_{21} + T_{12}R_{23}T_{21}(R_{21}R_{23}) + T_{12}R_{23}T_{21}(R_{21}R_{23})^{2} + \dots$$

Three-layers Reflection

$$R = R_{12} + T_{12}R_{23}T_{21} + T_{12}R_{23}T_{21}(R_{21}R_{23}) + T_{12}R_{23}T_{21}(R_{21}R_{23})^{2} + \dots$$

$$R = R_{12} + \sum_{n=0}^{\infty} T_{12} R_{23} T_{21} (R_{21} R_{23})^n$$

$$R = R_{12} + T_{12}R_{23}T_{21}\sum_{n=0}^{\infty} (R_{21}R_{23})^n$$

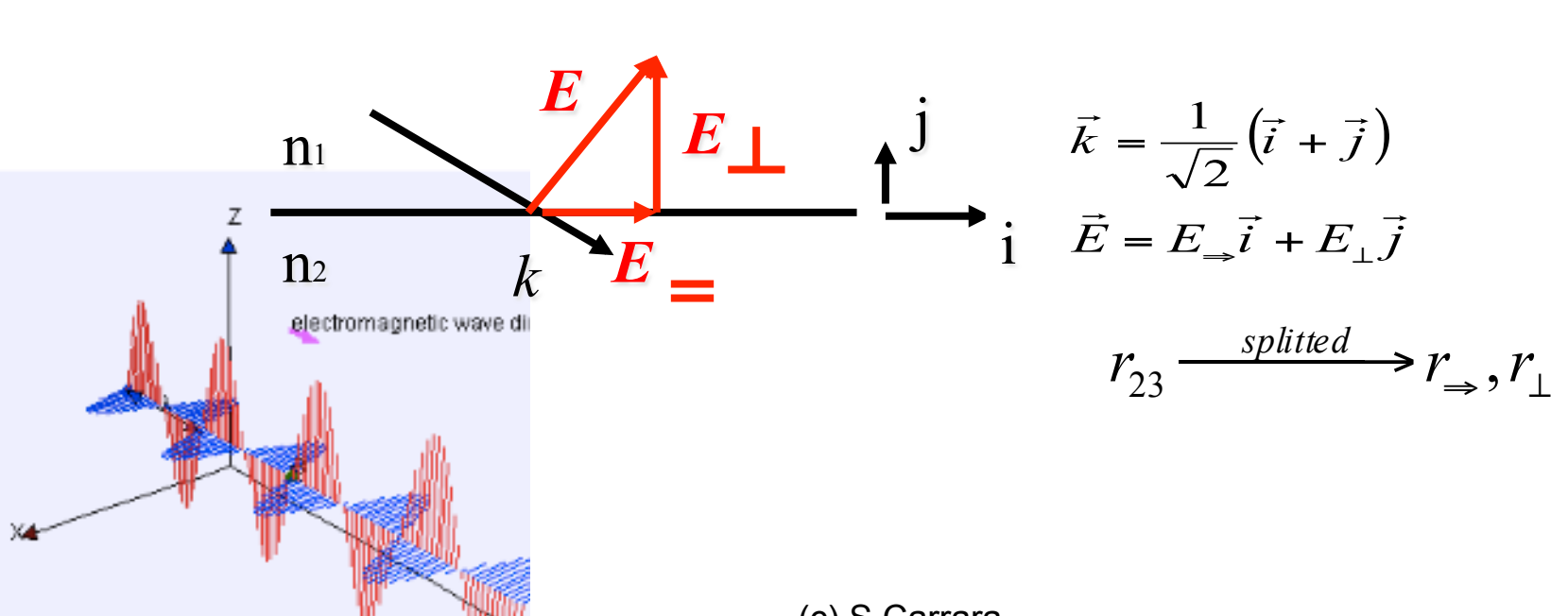
By the geometric series

$$\sum_{n=0}^{\infty} x^n = \frac{1}{1-x}$$

$$R = R_{12} + T_{12}R_{23}T_{21} \frac{1}{1 - R_{21}R_{23}}$$

The Reflection coefficient and the Electrical Field

$$R = R_{12} + \frac{T_{12}R_{23}T_{21}}{1 - R_{2}R_{23}} \qquad R_{23} = |r_{23}|^{2} \qquad R_{23} = \frac{I_{r}}{I_{i}}; r_{23} = \frac{E_{r}}{E_{i}}$$



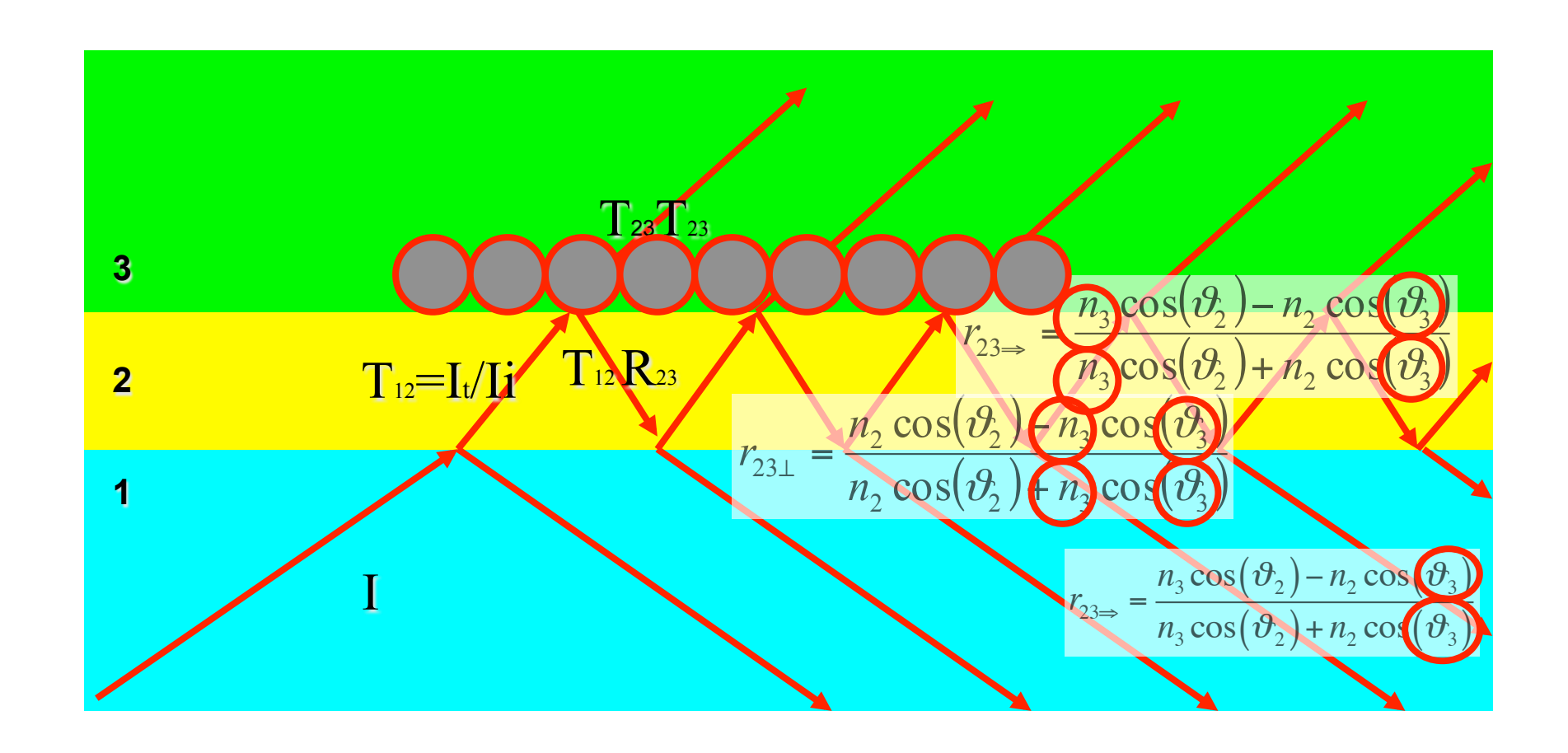
(c) S.Carrara

The Fresnel Coefficients

$$r_{23} \xrightarrow{splitted} r_{\Rightarrow}, r_{\perp}$$

$$r_{2$$

Three-layers Reflection



Product

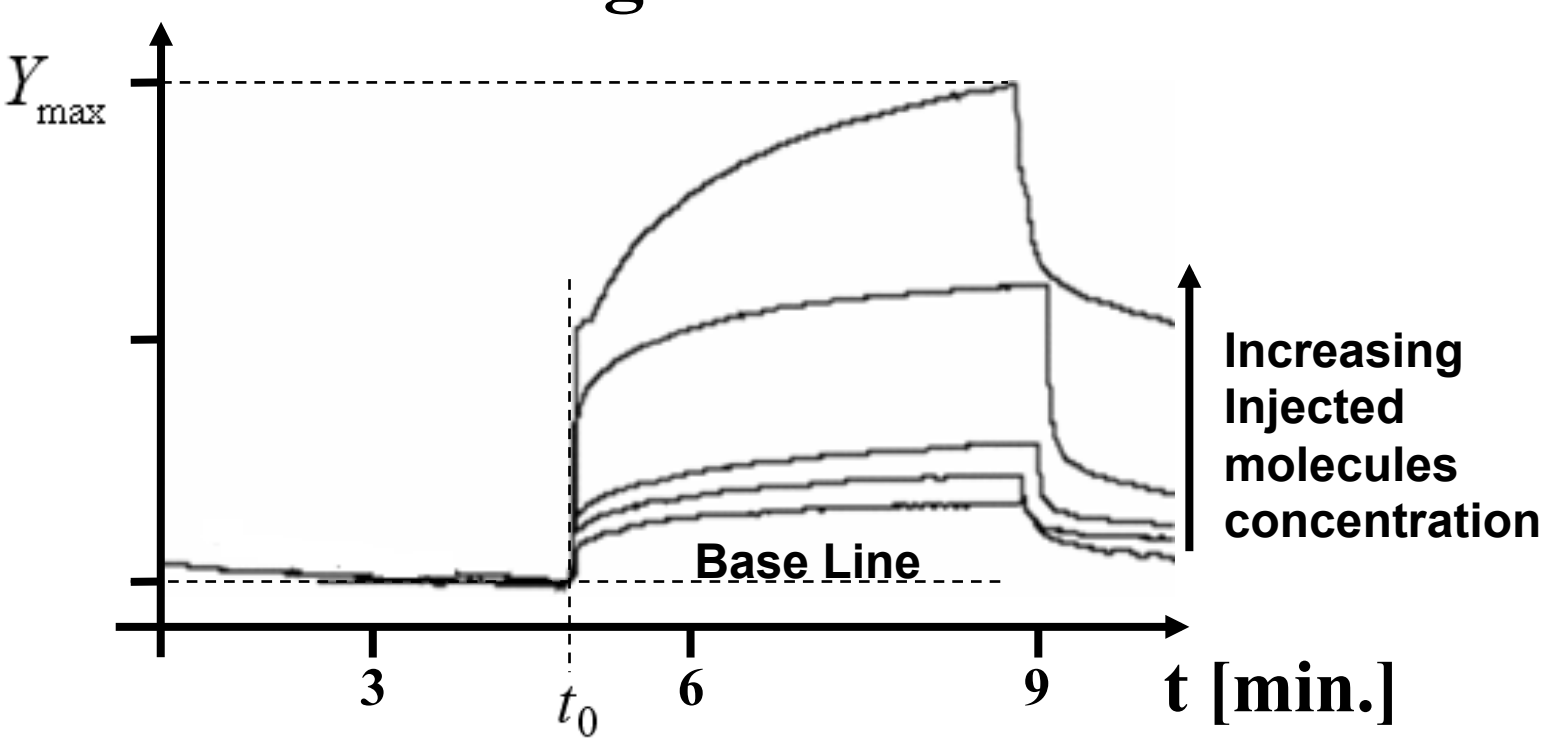


IAsys plus Affinity Sensor

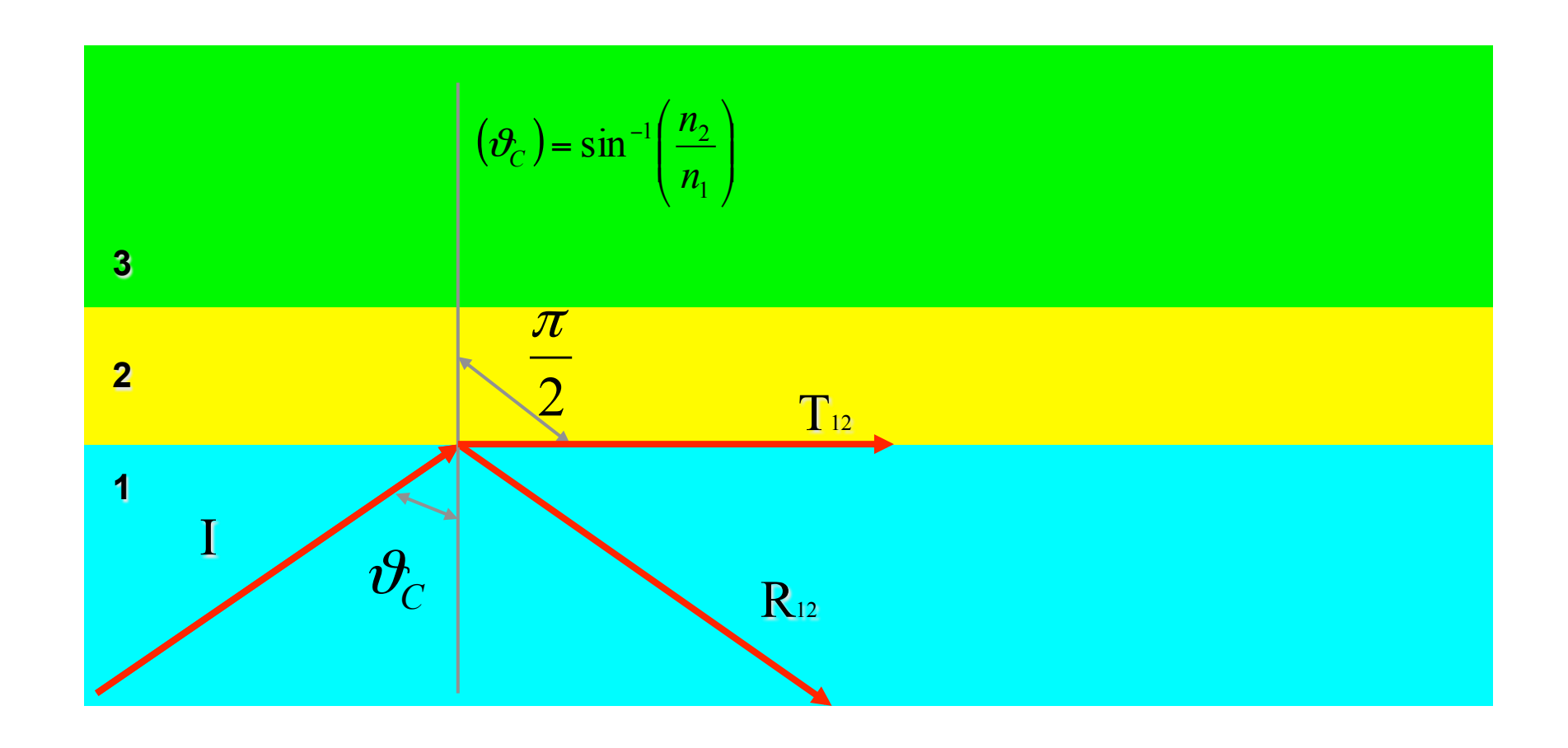
(c) S.Carrara

Yield Monitoring

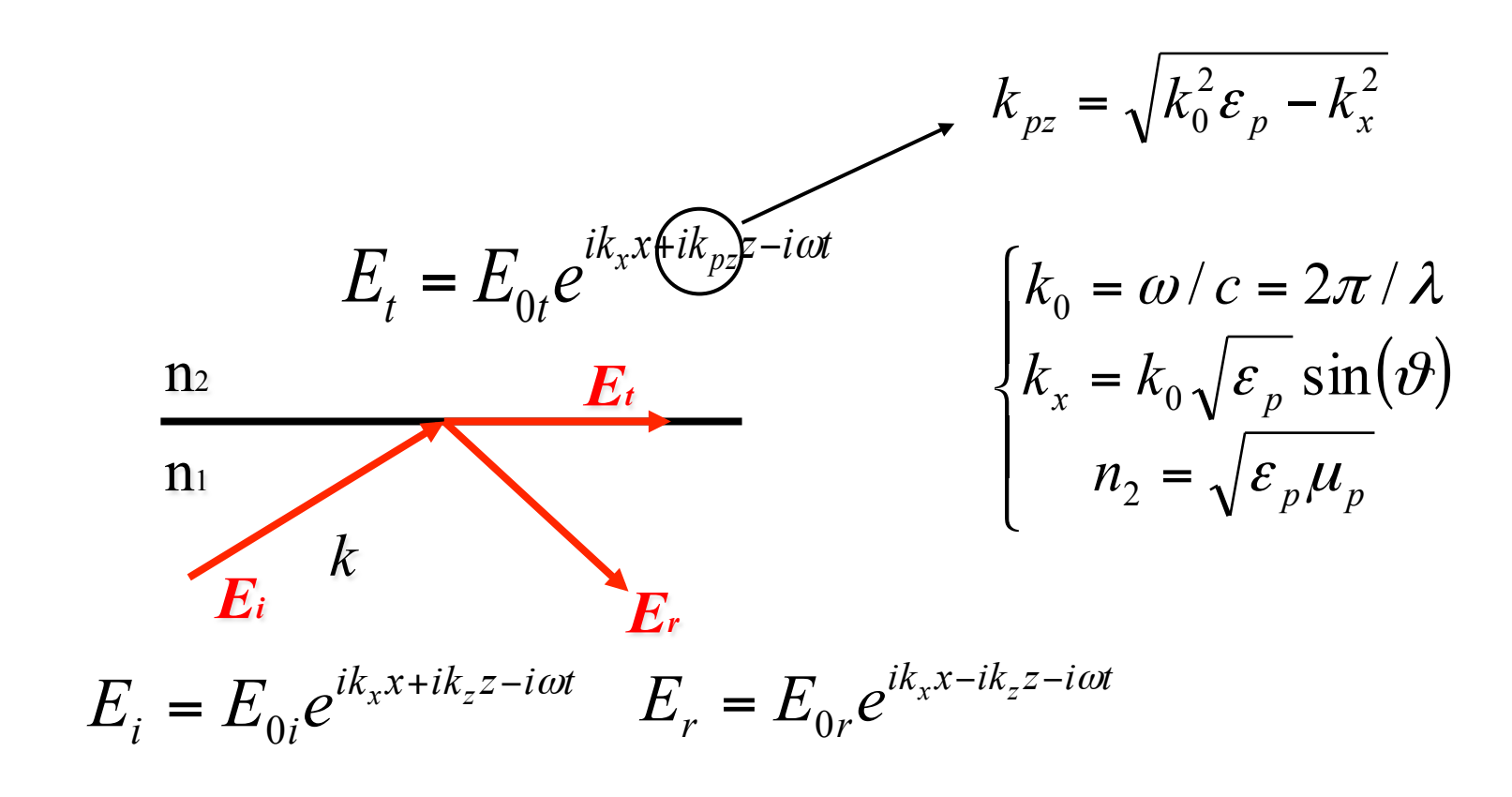
Yield = Percentage of covered surface



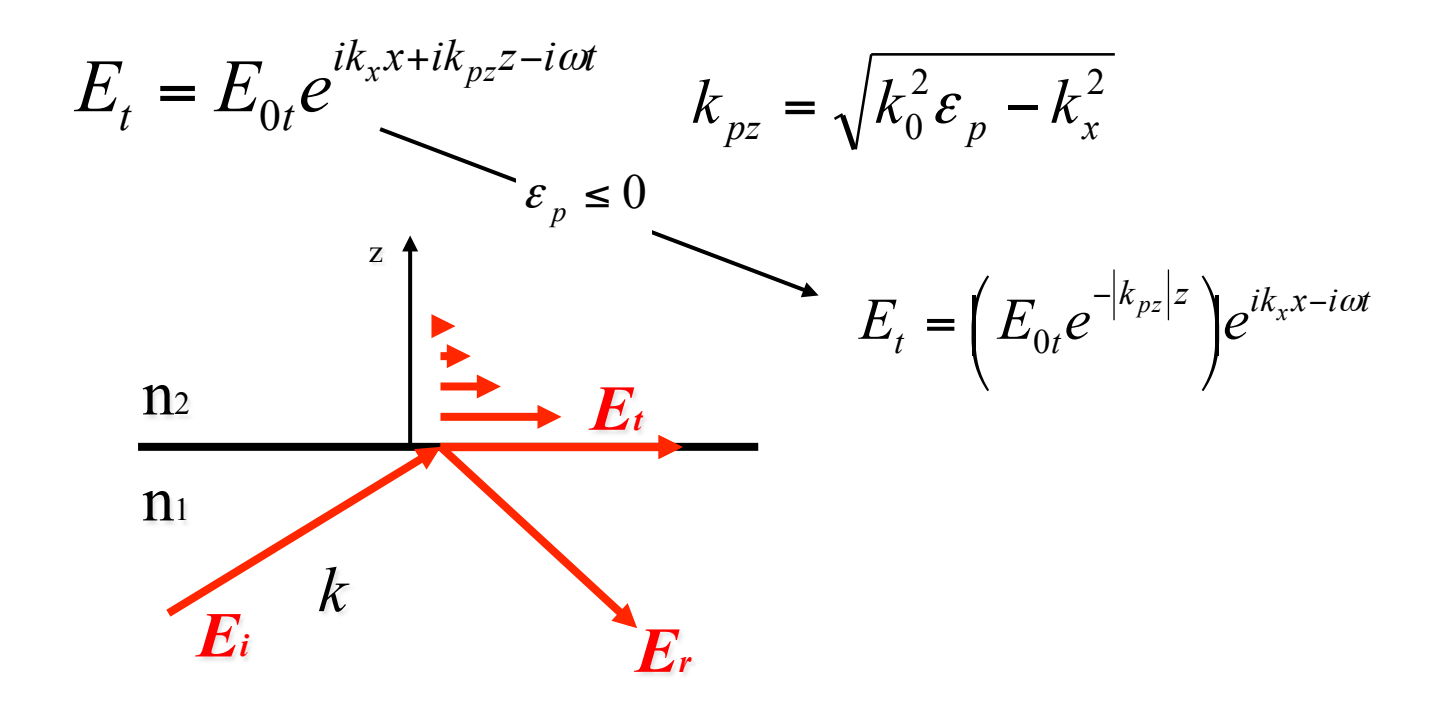
Three-layers Reflection



The Propagation along the interface

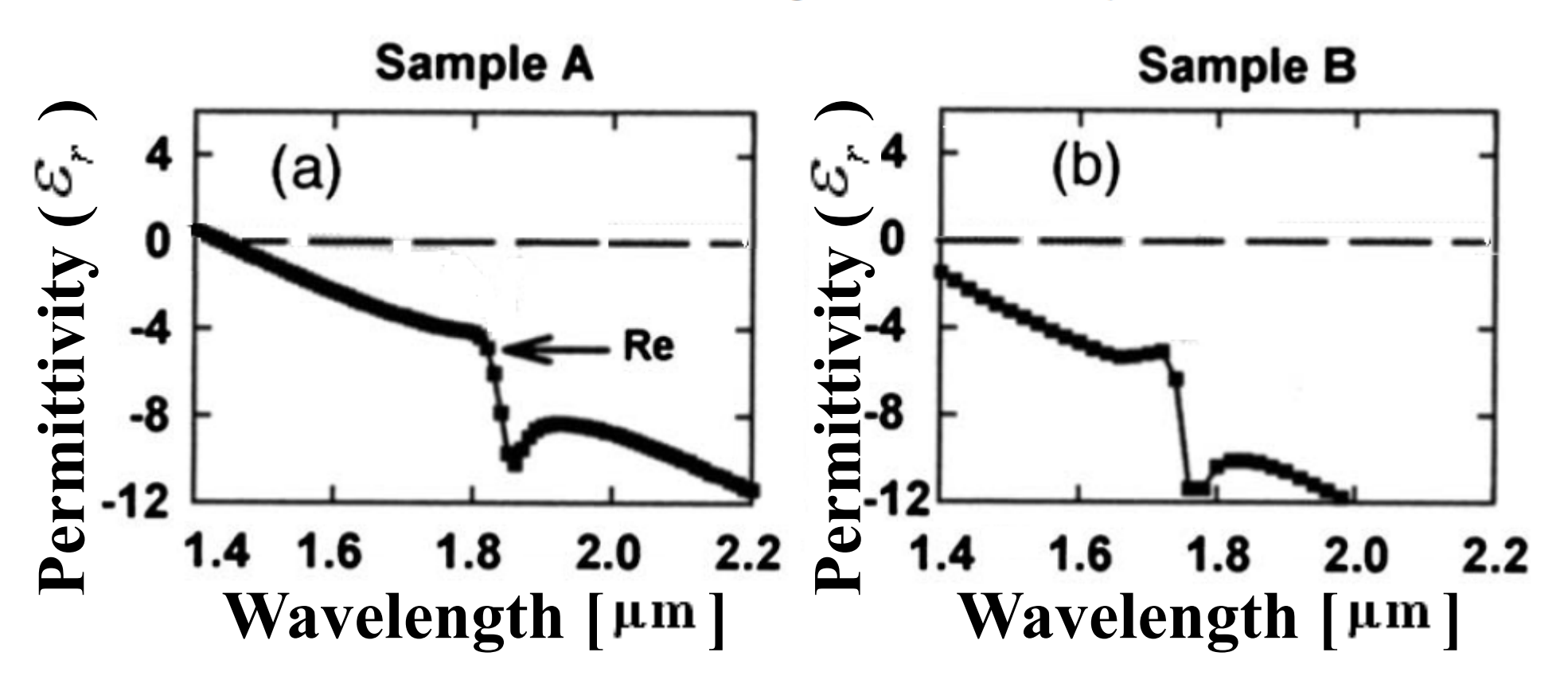


The Evanescent wave

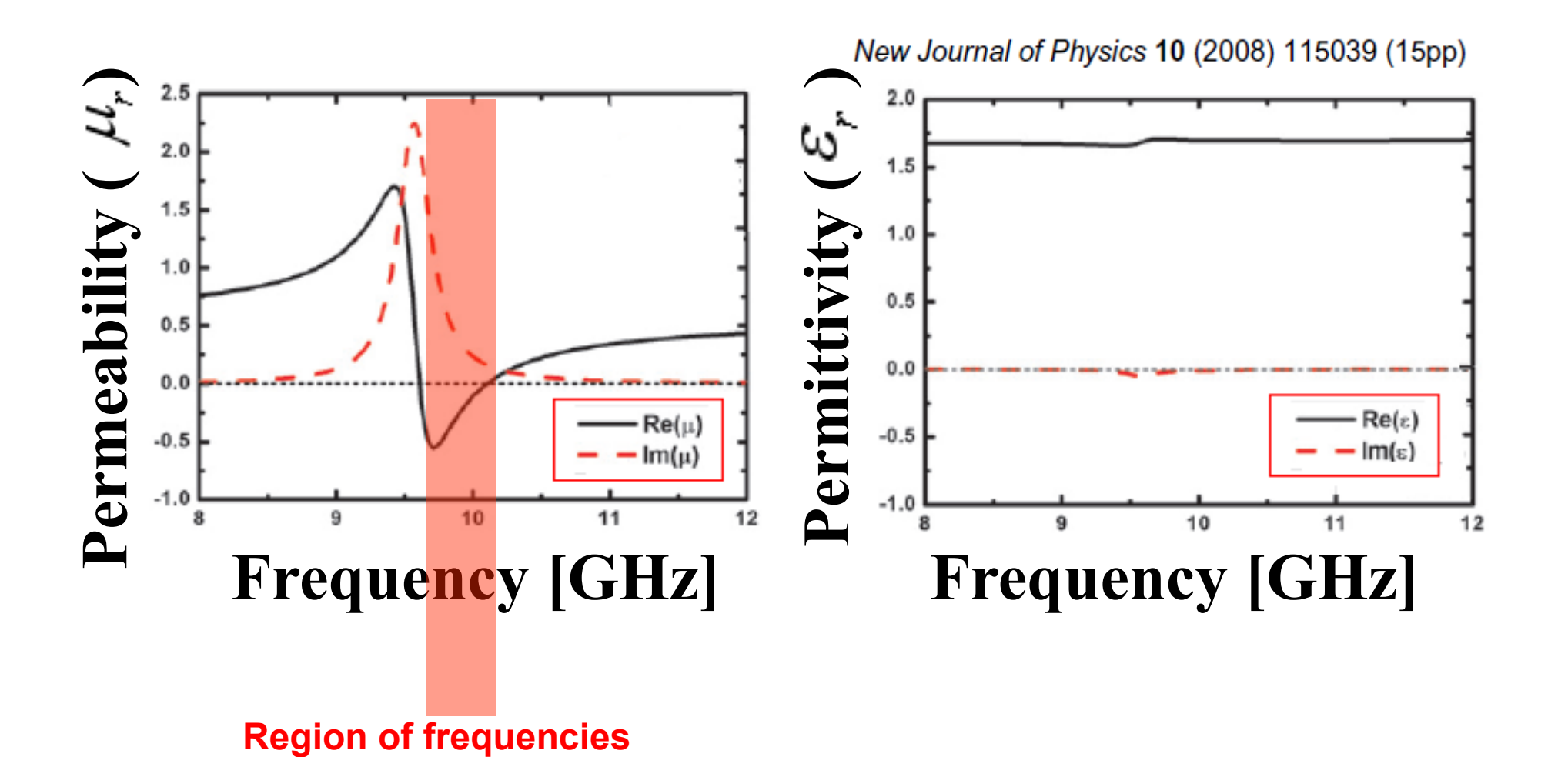


Negative Permeability of metals

Zhang et al. J. Opt. Soc. Am. B/Vol. 23, No. 3/March 2006 pag 434



Negative Permittivity in metallic clots



(c) S.Carrara

with negative permeability

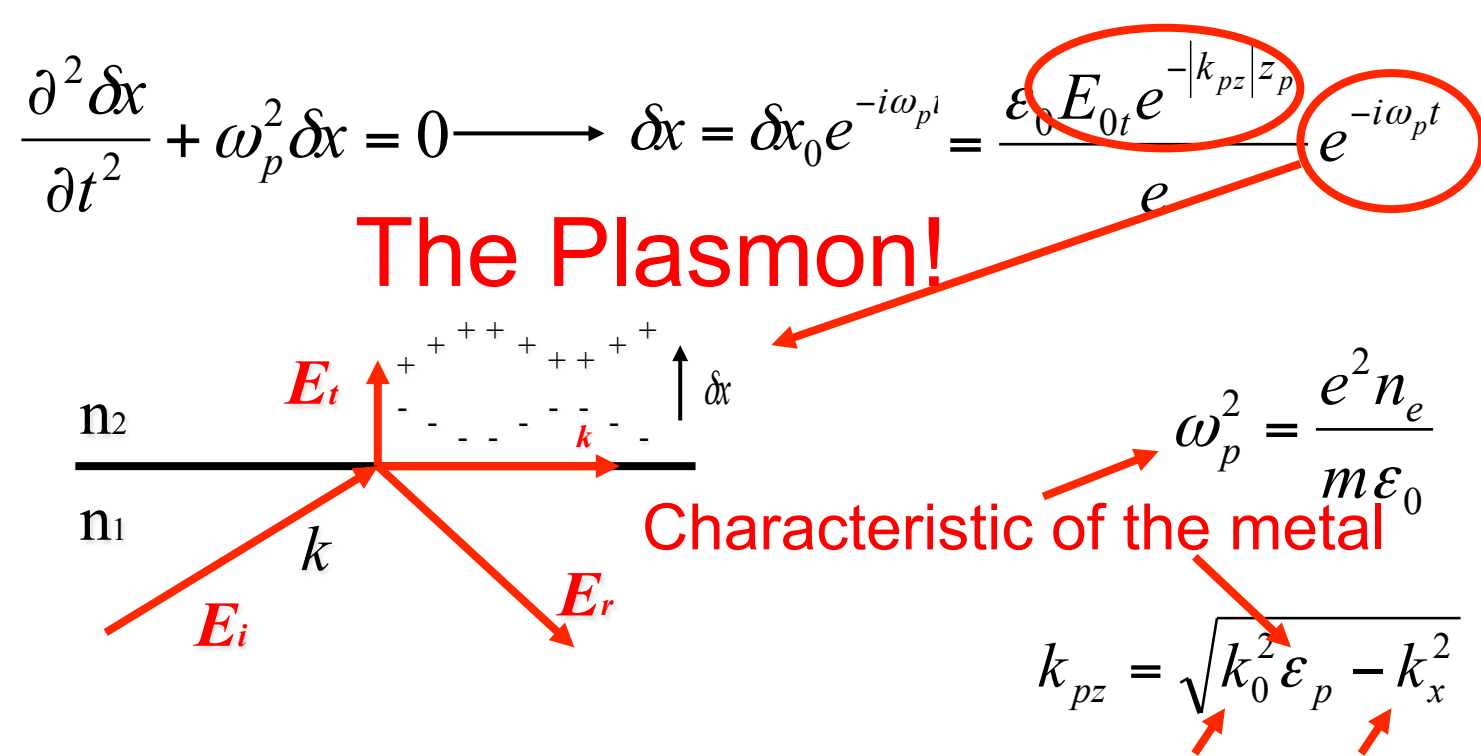
Negative dielectric constant

$$E_{t} = \left(E_{0t}e^{-|k_{pz}|^{2}}\right)e^{ik_{x}x-i\omega t} \qquad \qquad F = ma = m\frac{\partial^{2}\delta x}{\partial t^{2}}$$

$$F = eE_{t} = -eE_{\delta x} = -e\frac{\sigma}{\varepsilon_{0}}$$

$$E_{t} \qquad \qquad E_{t} \qquad \qquad E_{t$$

Electronic Waves



Characteristic of the evanescent wave

Simulation of Evanescent wave propagation

410 nm for HeNe laser in glass

Penetration of the Evanescent Wave

For an amplitude of 1/3 of the value in z=0, we have

$$E_{ot}e^{-|k_{mz}|z} = \frac{1}{3}E_t|_{z=0} = \frac{1}{3}E_{0t} \longrightarrow e^{-|k_{mz}|z} = \frac{1}{3} \approx \frac{1}{e}$$
By extracting z:
$$z = \frac{1}{|k_{mz}|} = \frac{c_0}{2\pi f \sqrt{|\mu_r \varepsilon_r|}} = \frac{\lambda}{\sqrt{|\mu_r \varepsilon_r|}}$$

For gold, with relative magnetic permeability close to one and relative electric permittivity equal to 6.9, we obtain a thickness of

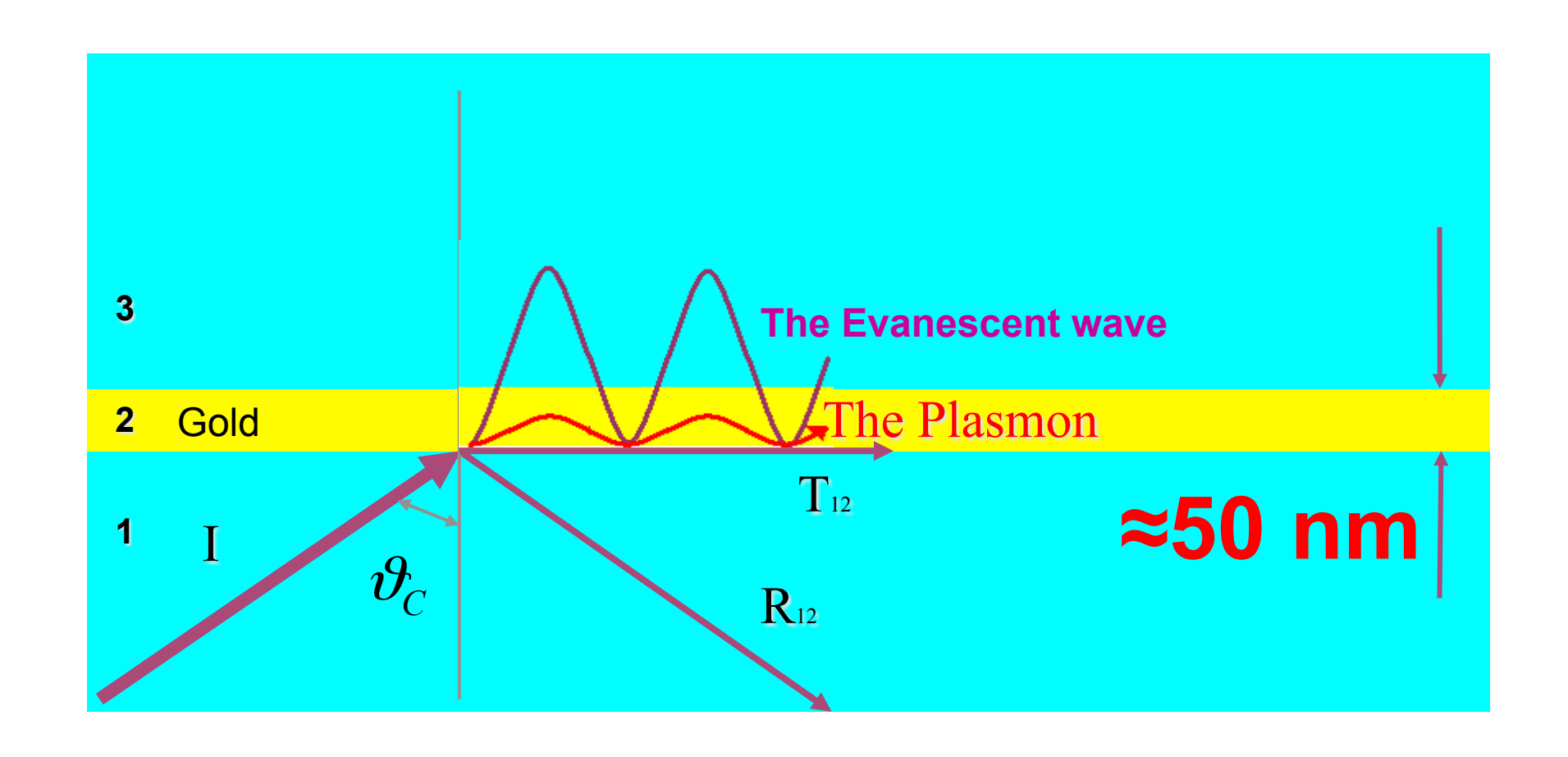
$$z_{gold} = \frac{1}{|k_{mz}|} = \frac{\lambda}{\sqrt{|\mu_r \varepsilon_r|}} = \frac{400 \, nm}{\sqrt{6.9 \cdot 1}} \approx 152 \, nm.$$

For nickel, with permeability and permittivity equal to 100 and 10 (respectively), we get:

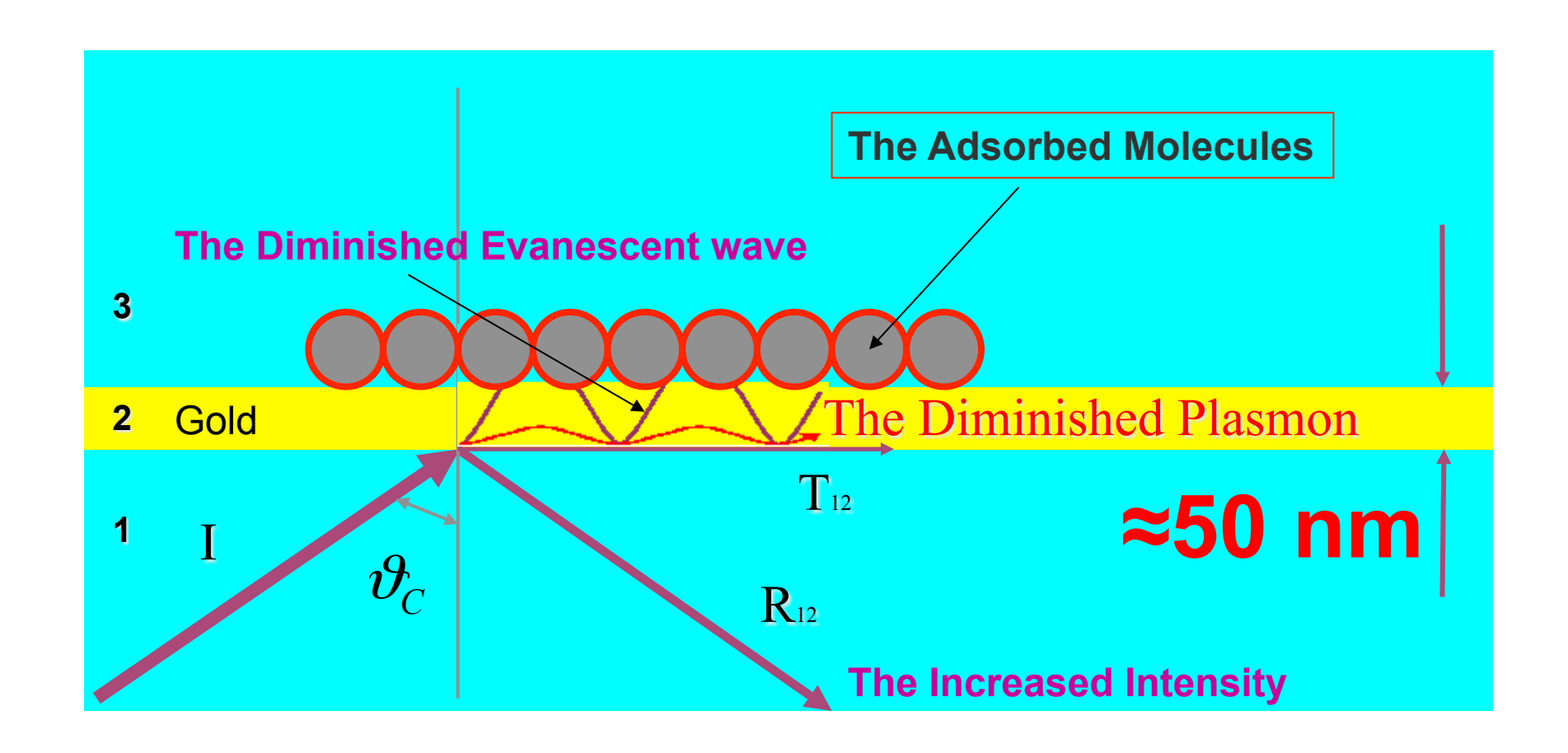
$$z_{nickel} = \frac{1}{|k_{mz}|} = \frac{\lambda}{\sqrt{|\mu_r \varepsilon_r|}} \approx \frac{400 \, nm}{\sqrt{100 \cdot 10}} \approx 12 \, nm.$$

(c) S.Carrara

Penetration of the Evanescent Wave



Perturbation of the Evanescent Wave

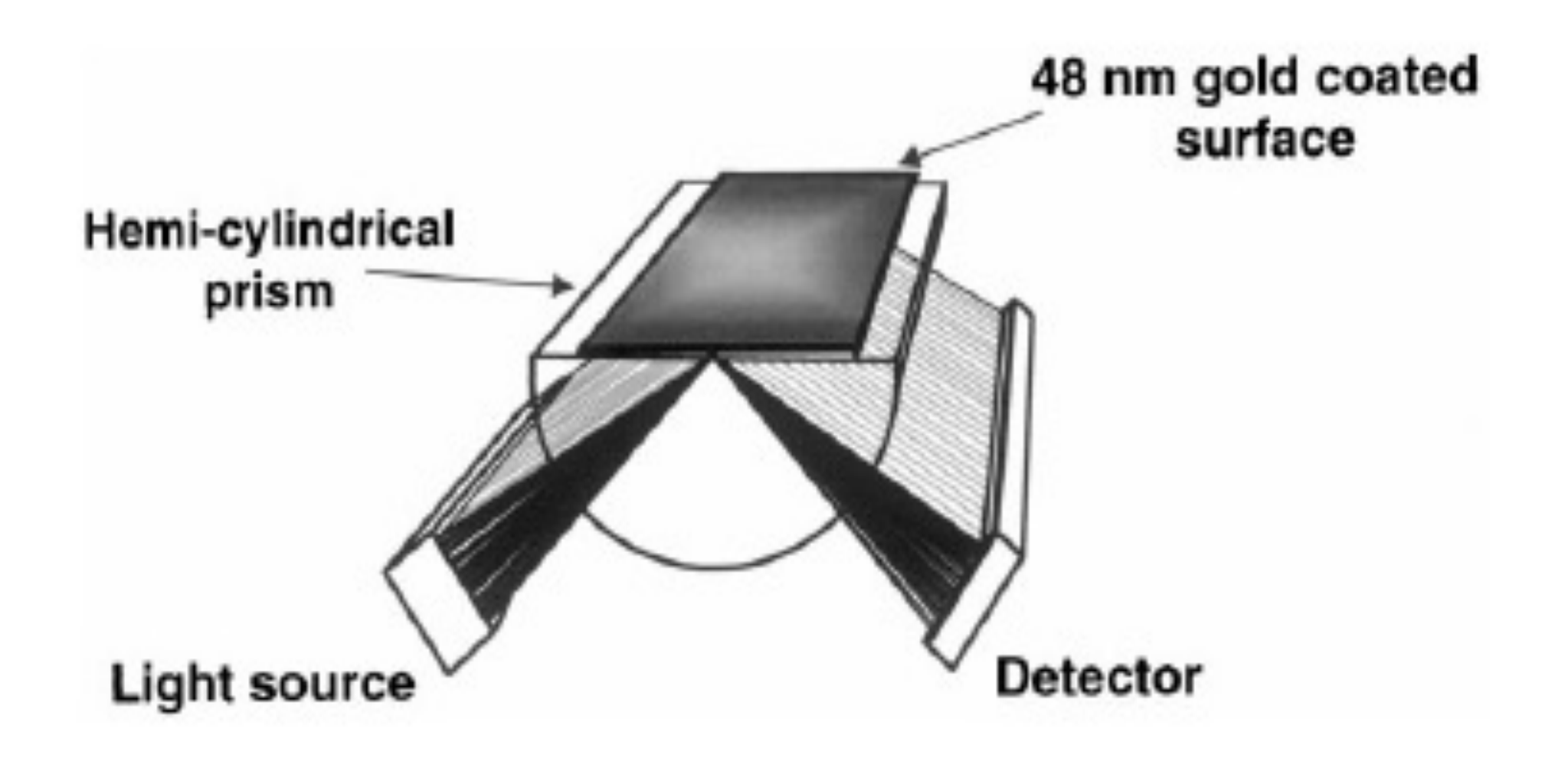


A Plasmon Resonance based Biosensor

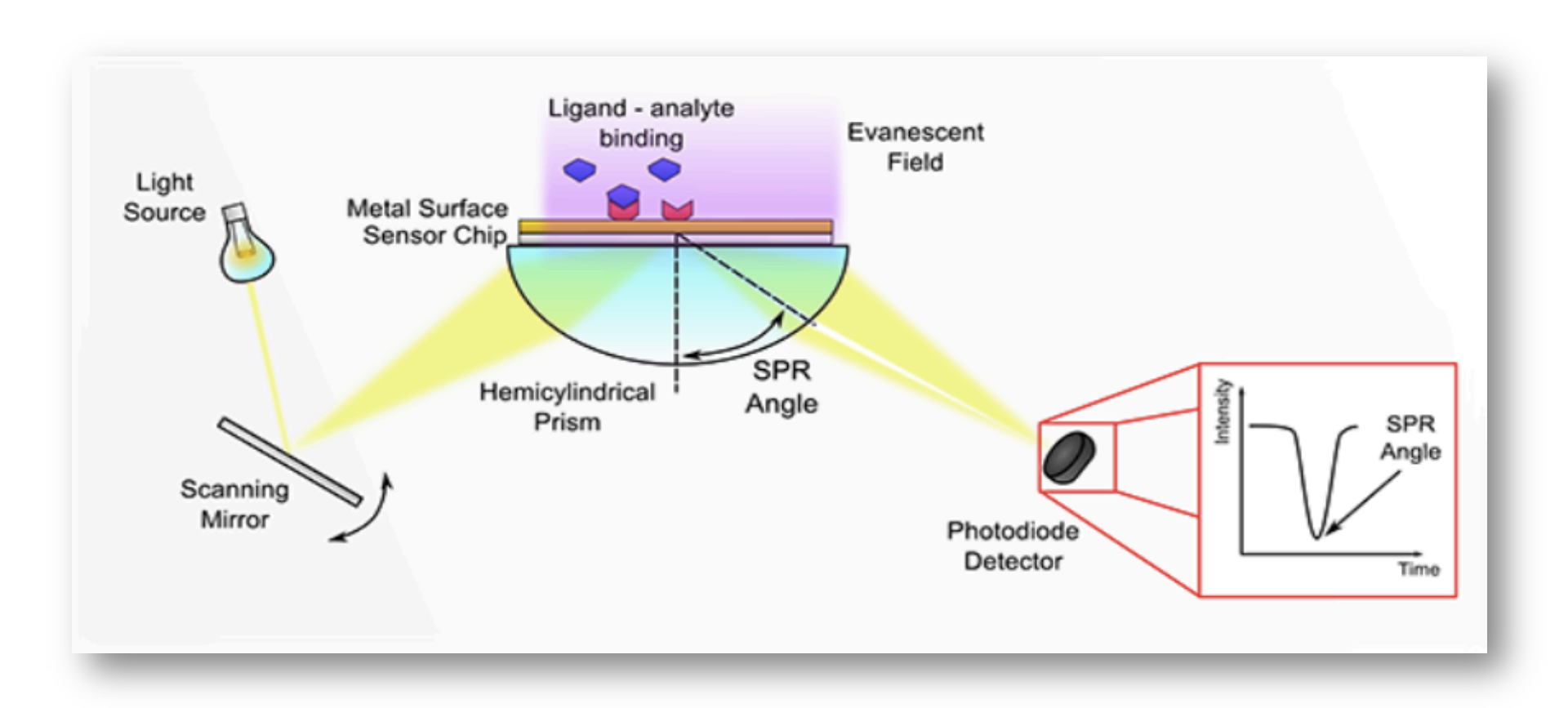


BIACORE 3000

The sensing Area

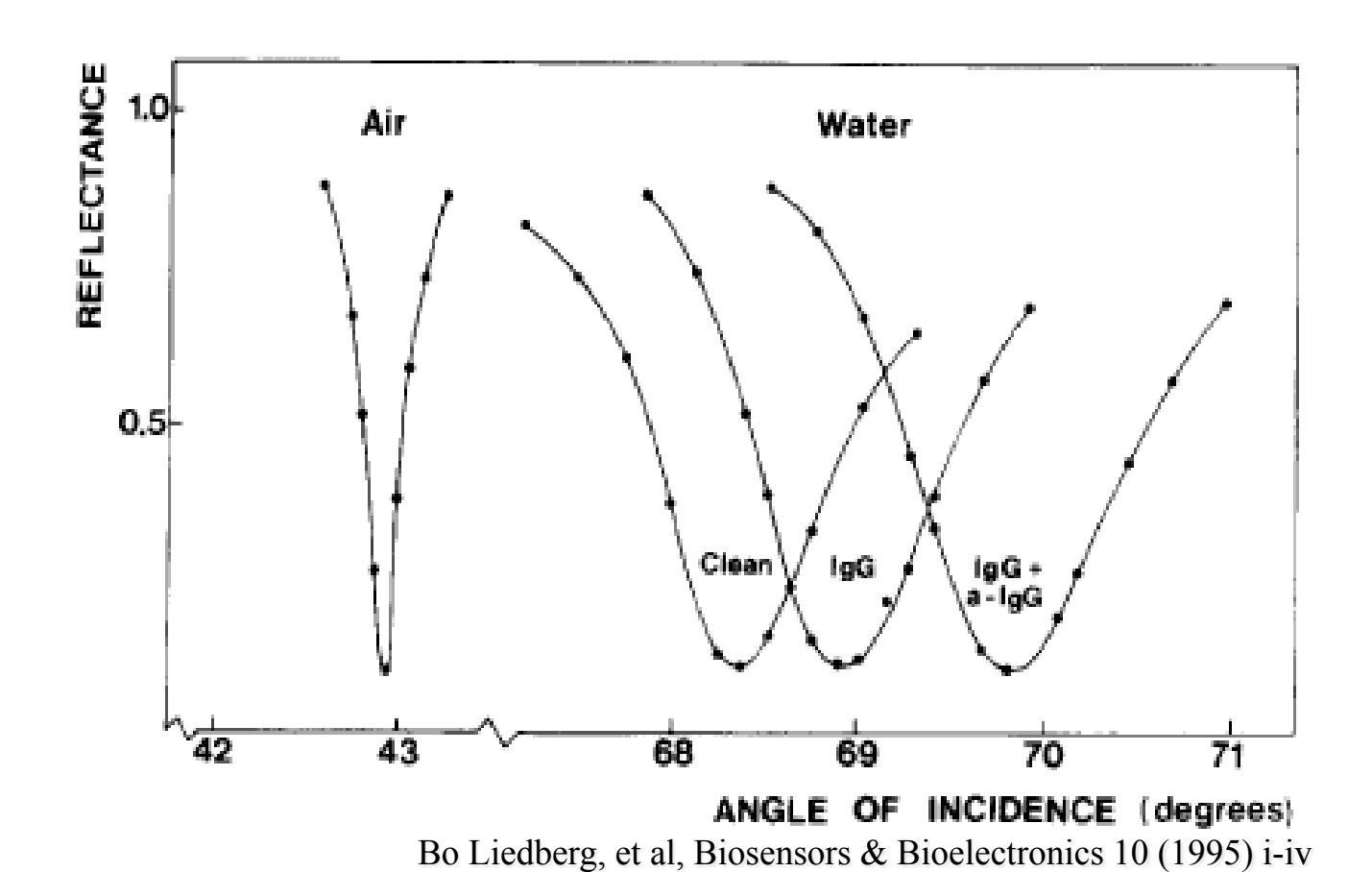


Working Principle



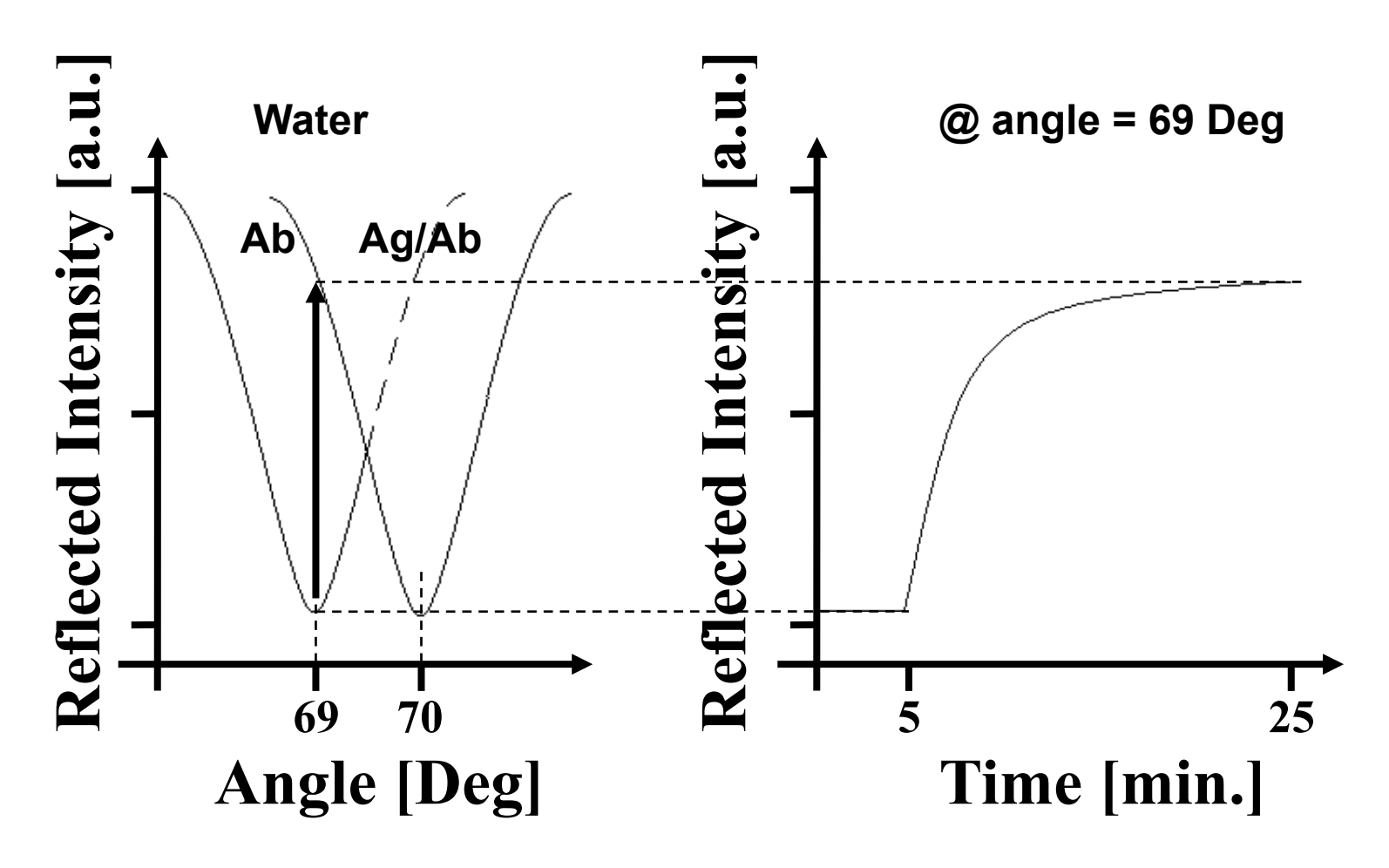
The persence of the complexes onto the gold surface will change the angle of resonance for the formation of the Surface Plasmons. This shift is proportional to the ligands amount bonded onto the surface

Characterization of Monoclonal antibodies



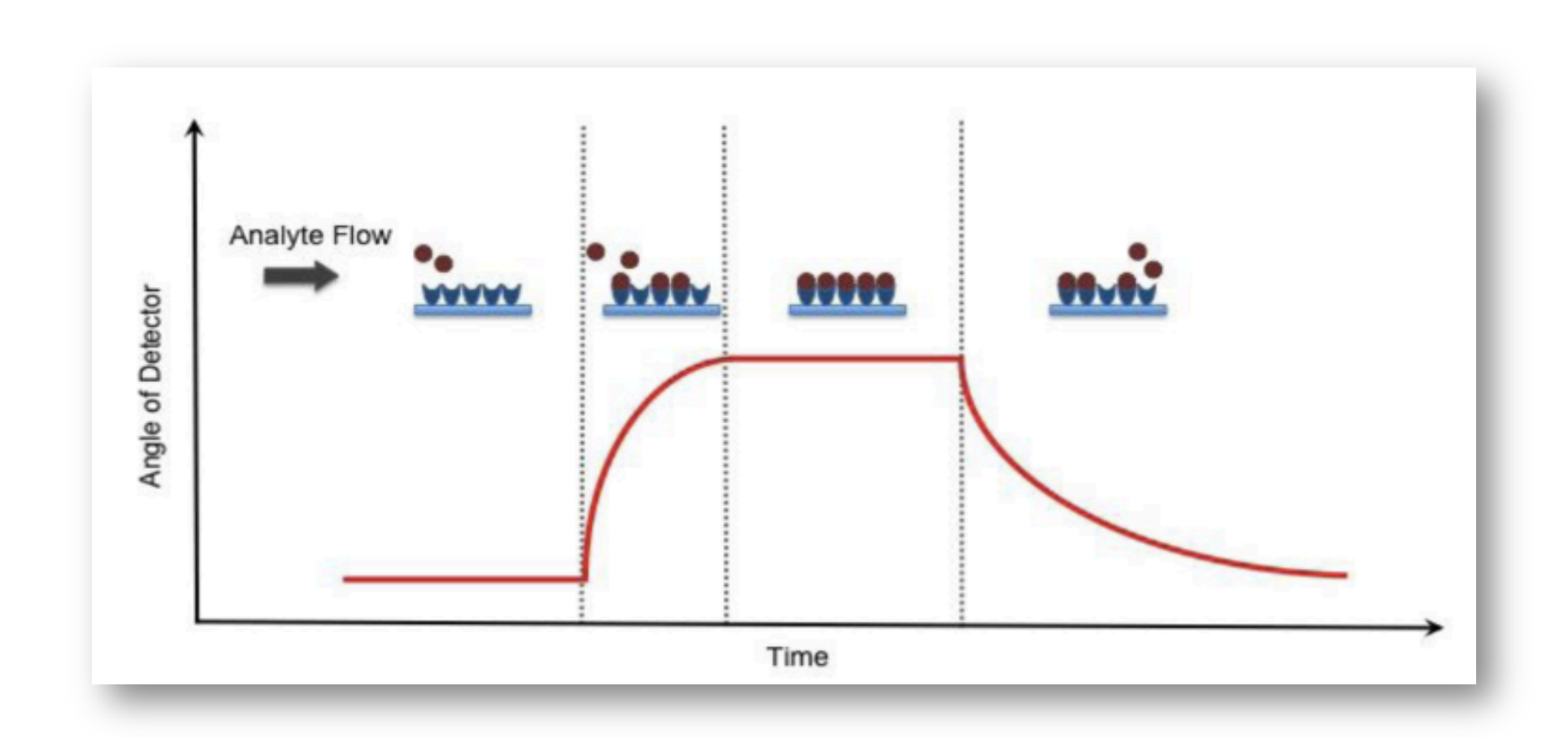
Shift in the resonant angle to sense IgG adsorption

Kinetic Studies



The kinetics could is reached by means of the change of the reflected intensity at fixed angle

Detection of Binding Events



Molecular uptake as monitored by SPR

SPR on SAM

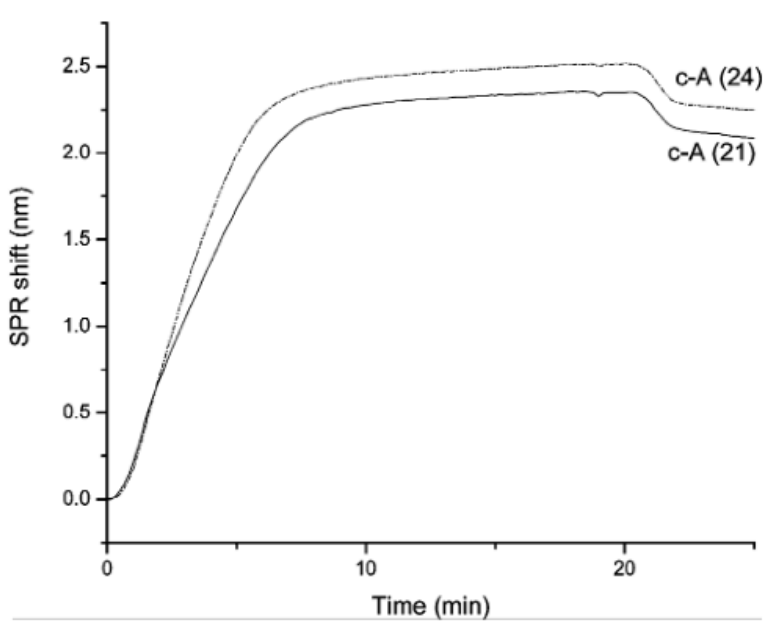


Figure 7. Comparison of the hybridization of a truncated complement (c-A 21) with the hybridization of the full-length complement (c-A 24). The ssDNA/OEG surface was prepared from a solution with a DNA mole fraction of 0.02.

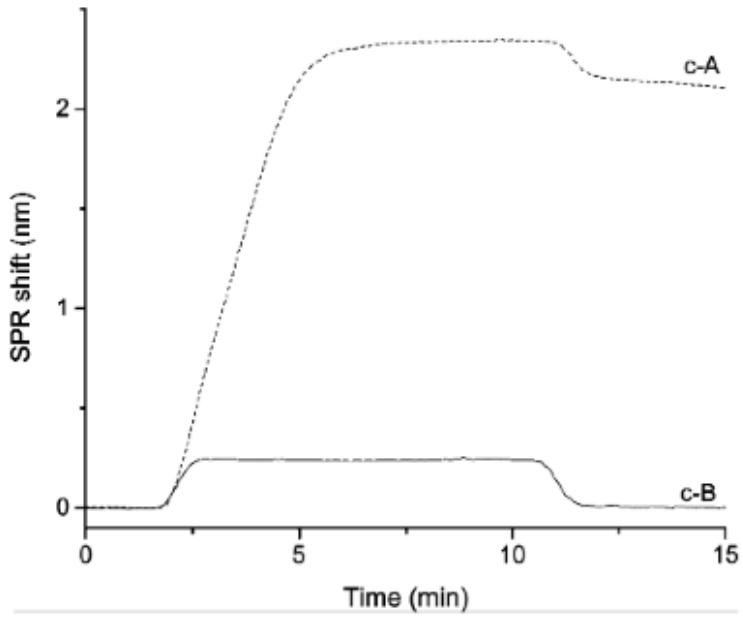


Figure 2. Control experiment to test DNA specificity. Both c-A and c-B were flowed over a sequence A ssDNA/OEG SAM, but only the complementary DNA hybridized. The ssDNA/OEG surface was prepared from a solution with a DNA mole fraction of 0.02.

Langmuir, Vol. 22, No. 10, 2006

DNA hybridization as monitored by SPR

SPR on SAM

Langmuir, Vol. 14, No. 11, 1998

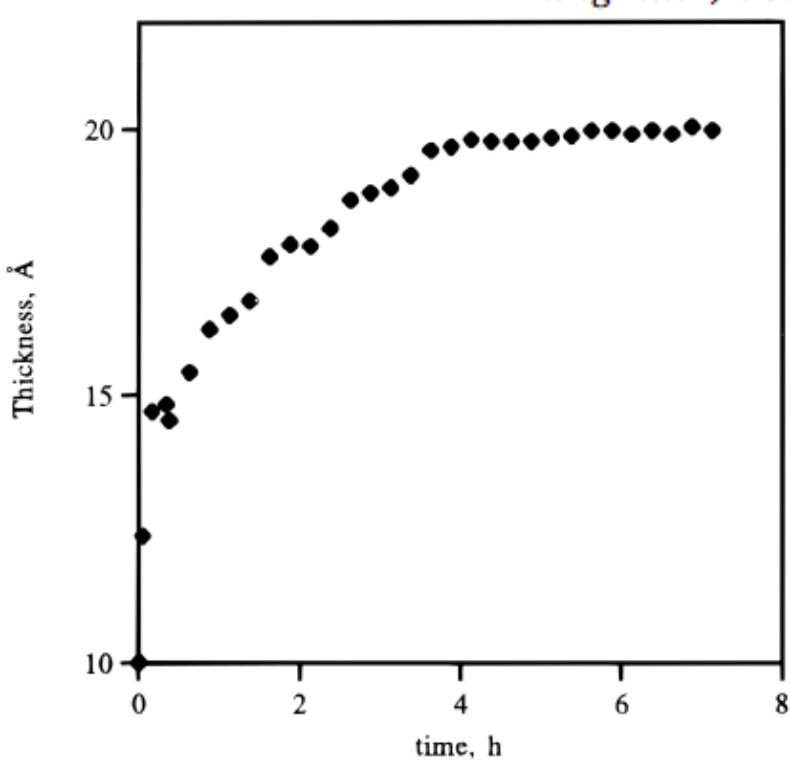


Figure 7. Increase in SPR measured thickness of the monolayer of disulfide **1** upon treatment with 0.1 mM ethanol solution of octadecanethiol.

Thiols SAM formation as seen by SPR

How to characterize the Probes Immobilization?

We have seen what are the mechanisms of self-assembly!

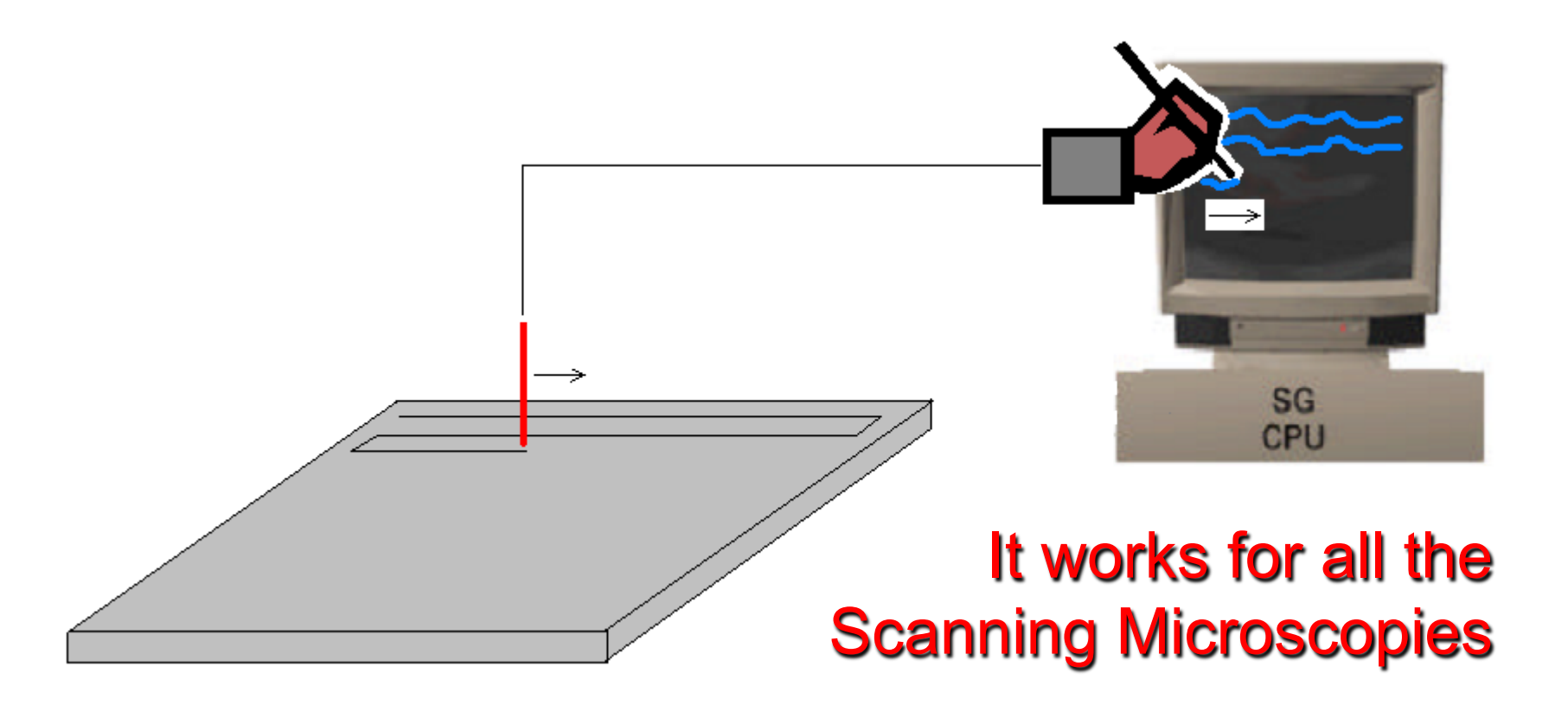
How to monitor the self-assembly process?

How to check the film quality?

Four different Microscopies

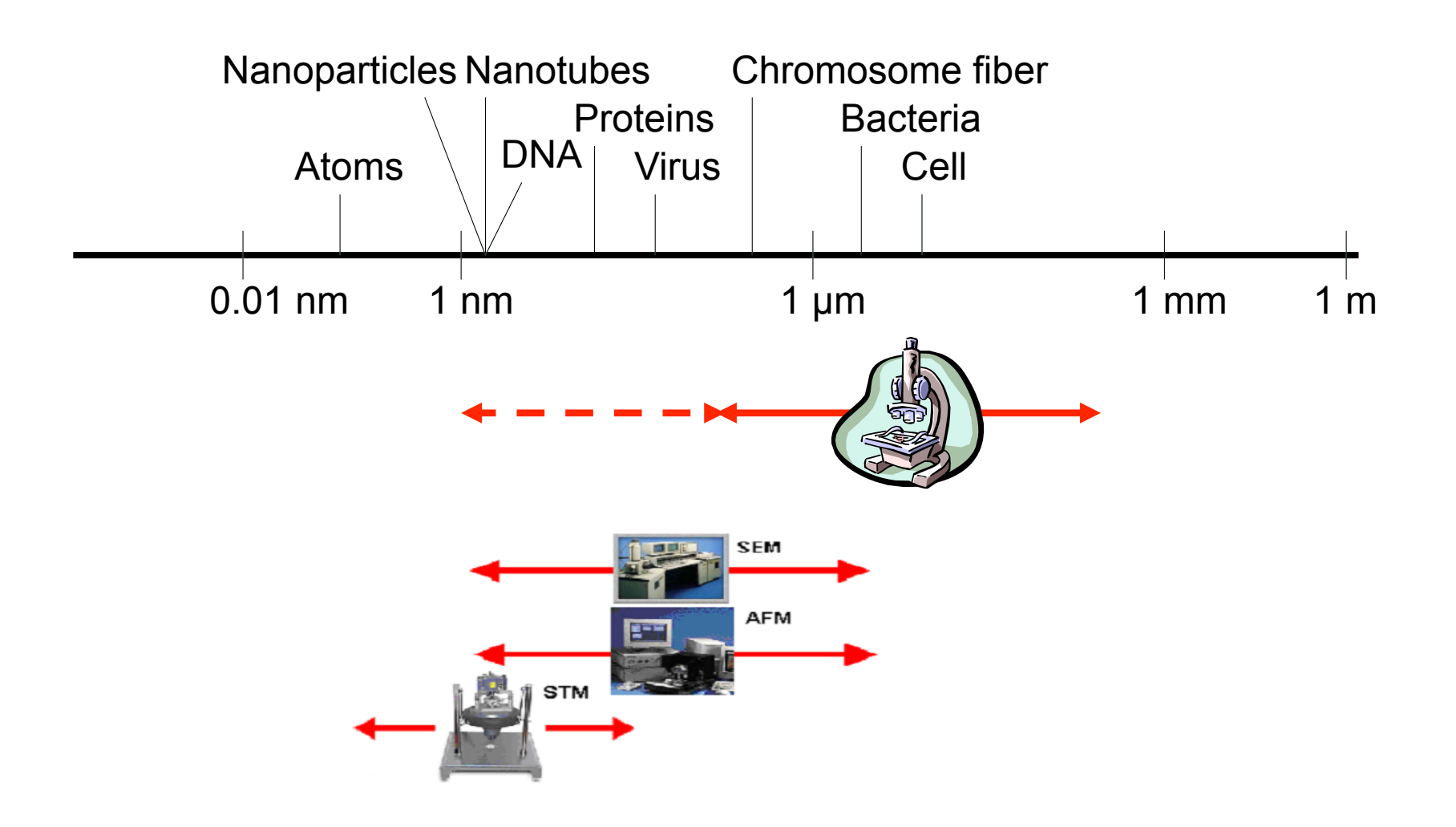
- 1. Transmission Electron Microscopy (**TEM**)
- 2. Scanning Electron Microscopy (SEM)
- 3. Atomic Force Microscopy (**AFM**)
- 4. Scanning Tunneling Microscopy (STM)

All are Scanning Microscopies



The sample scanning generates an image visualized with computer graphic tools

SEM Microscopy



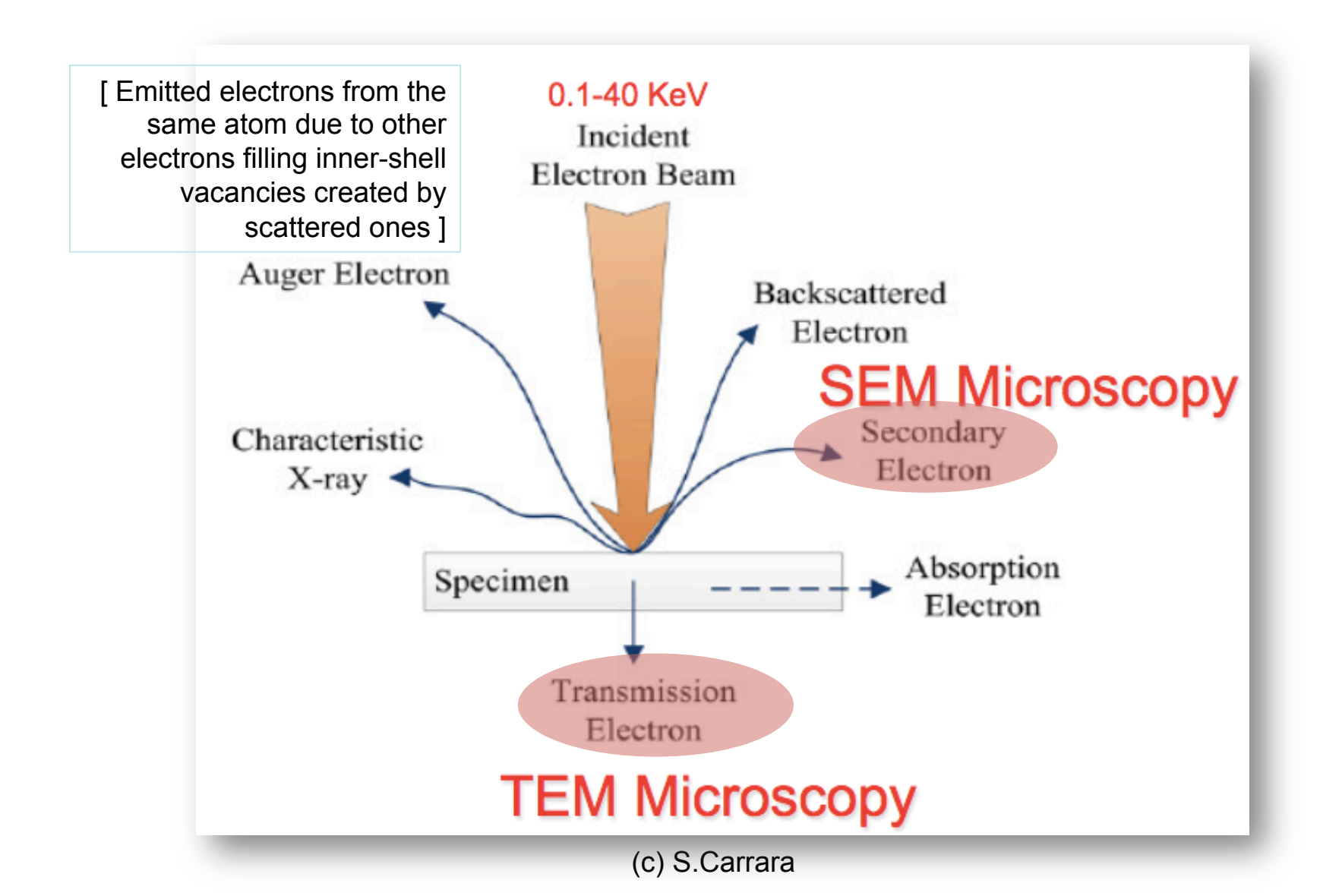
Electron Microscopies



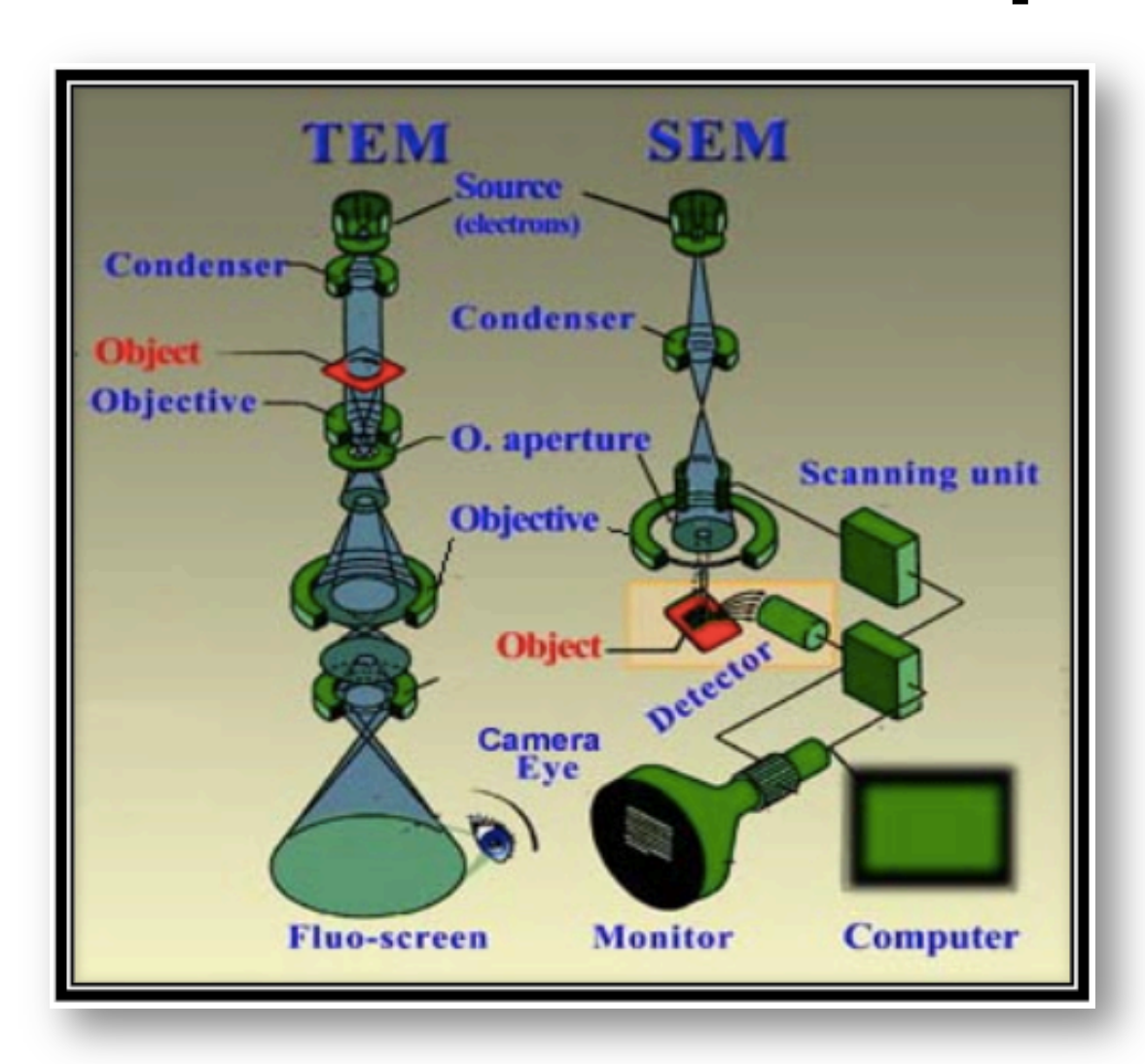
Transmission Electron Miscroscopy



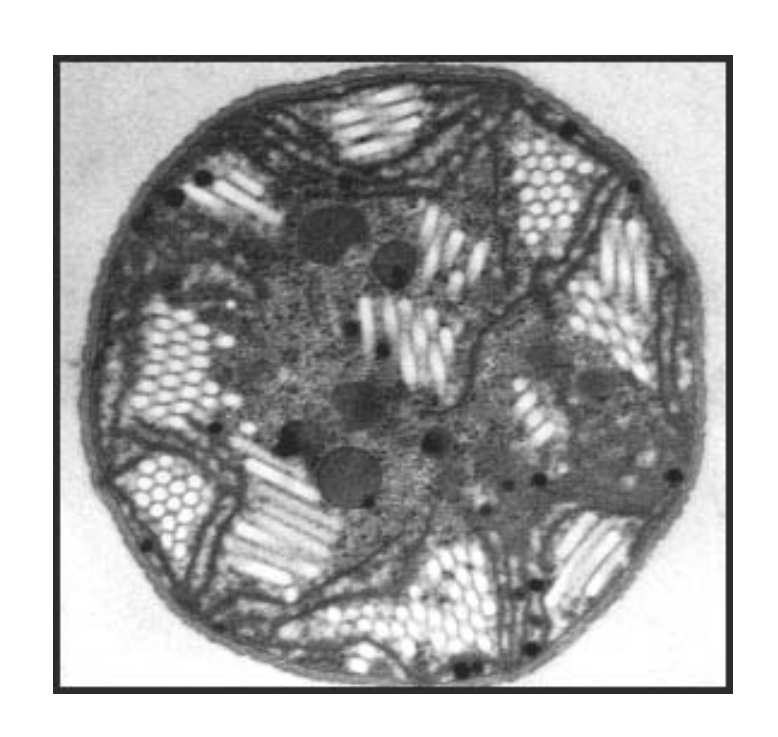
Electron Microscopy Principle



Electron Microscopies

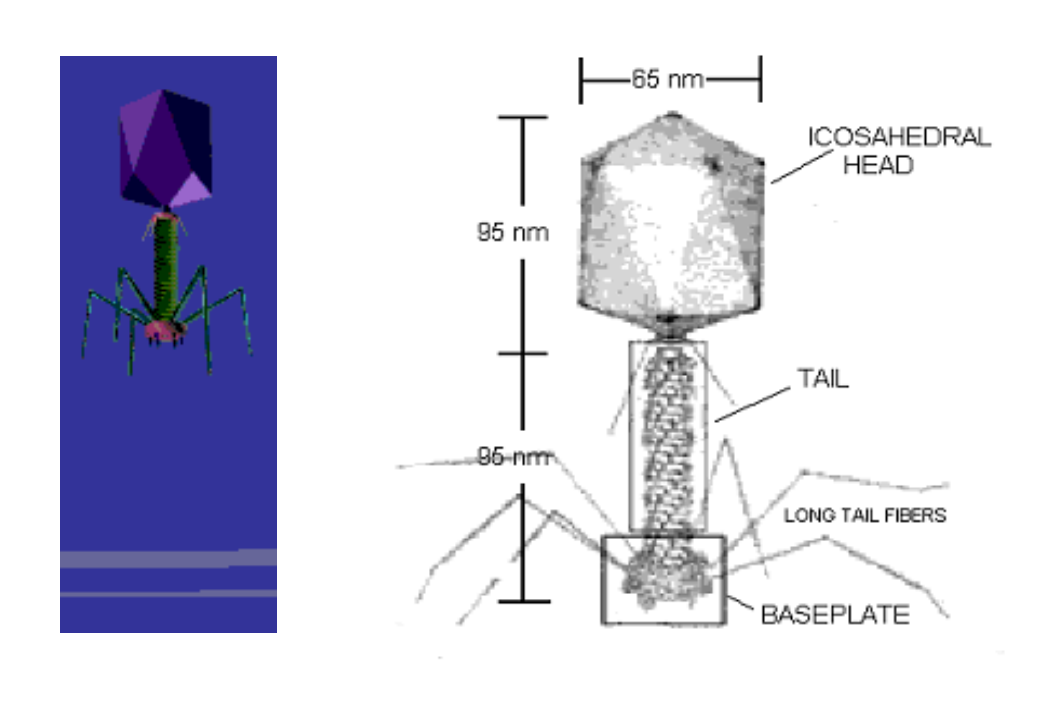


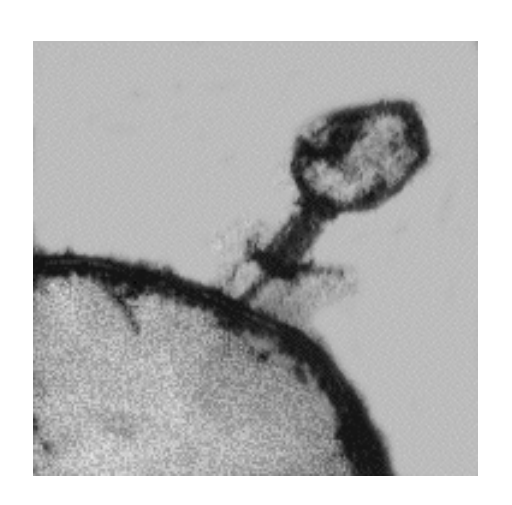
TEM Imaging



Cell of Cyanobacteria Microcystis by TEM

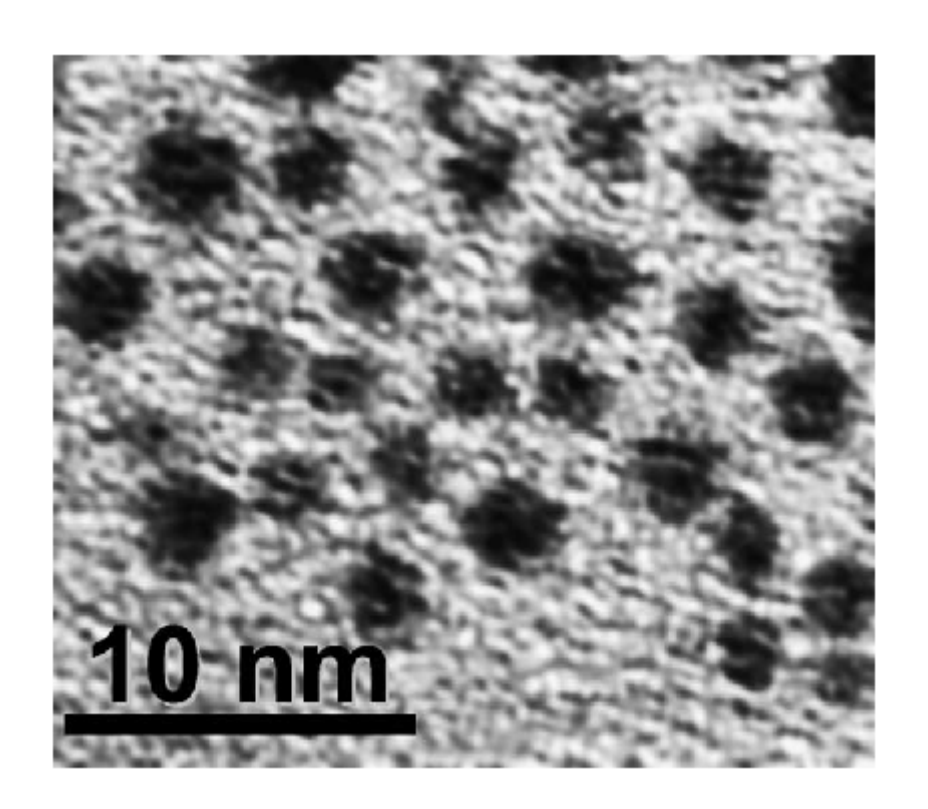
TEM Imaging





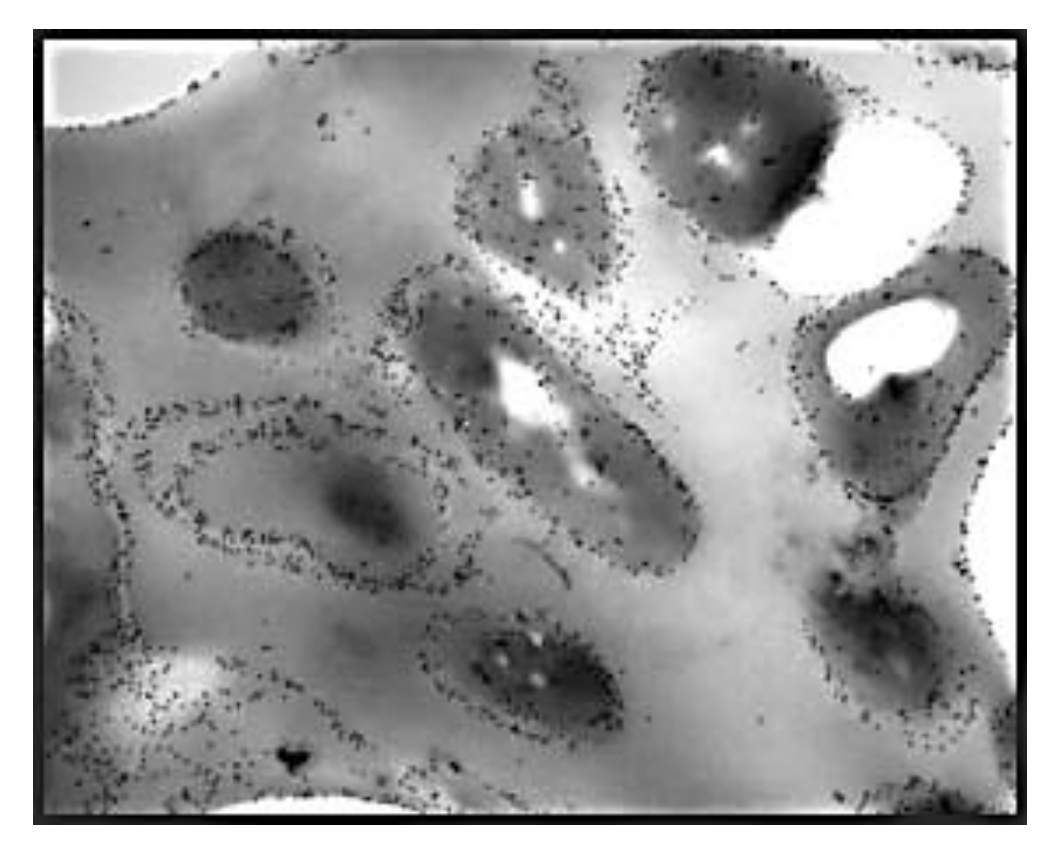
Virus T4 Bacteriophages

SEM Imaging

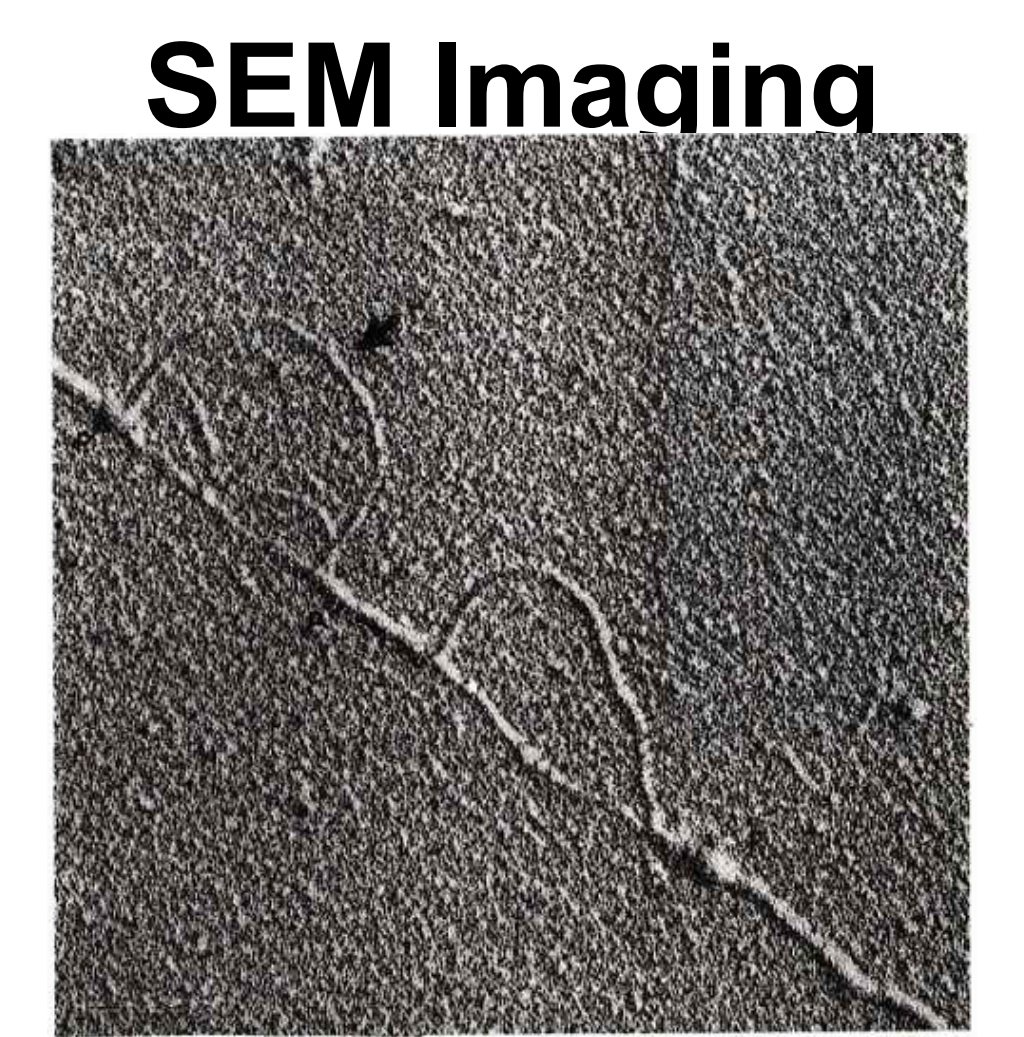


Gold nanoparticles made off gold core and a thiols-shell to stabilize the particle

SEM Imaging

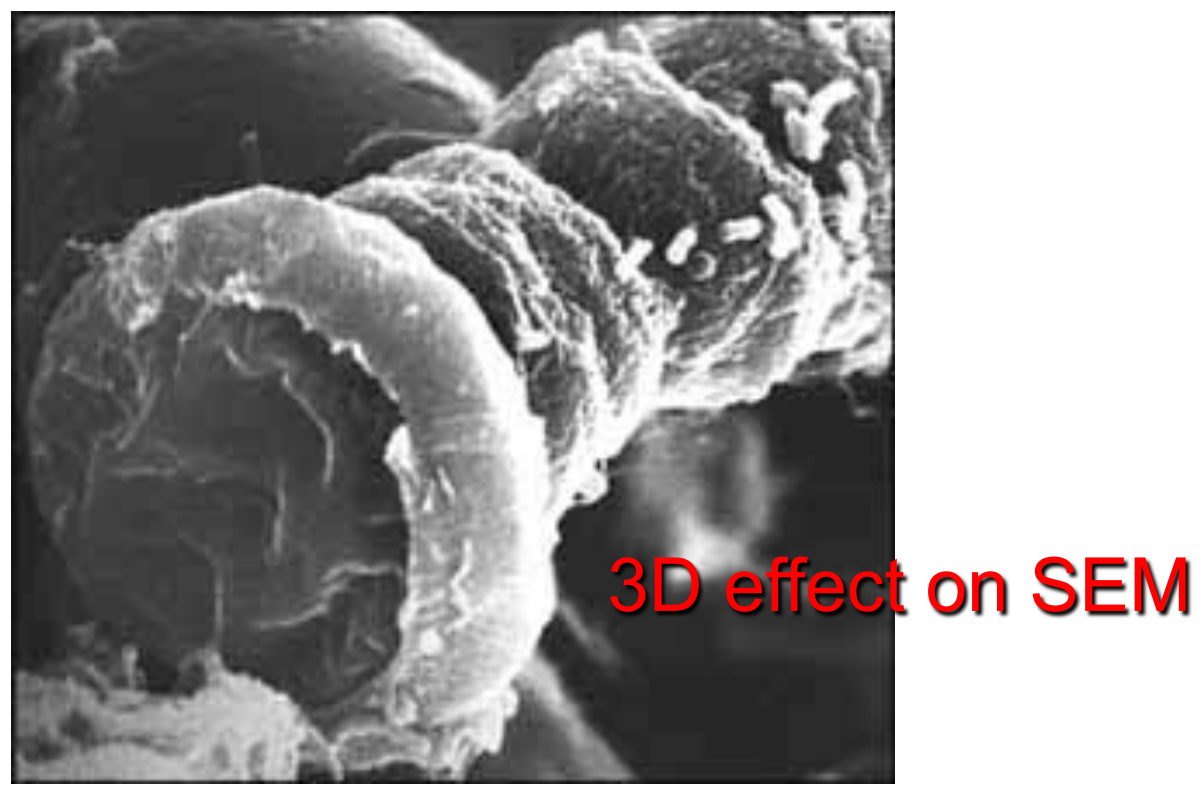


Antigens localized on the surface of bacteria cells



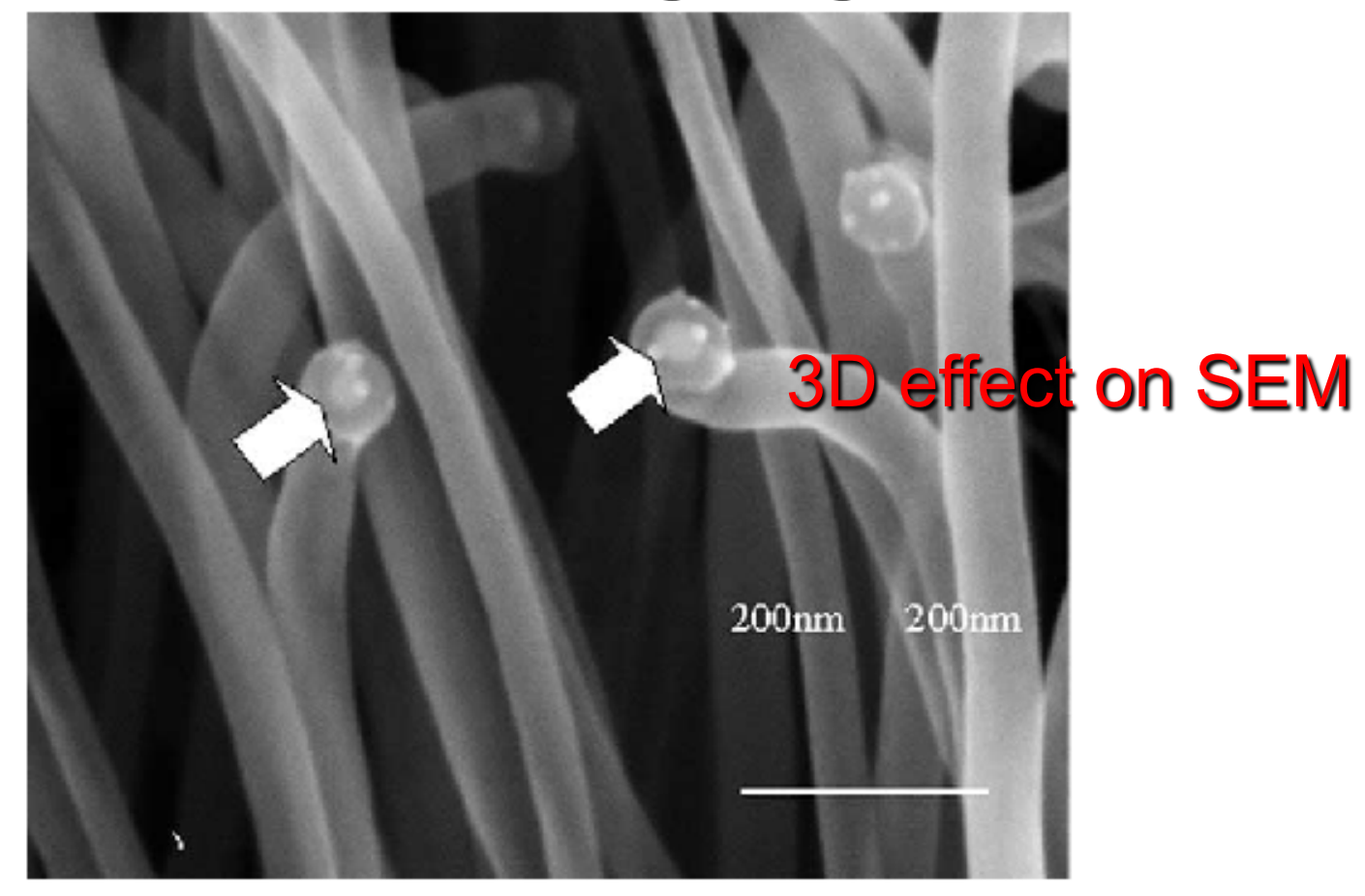
Isolated Chromatin (DNA-macromolecules including hystons and not-histons proteins) of about 30 nm and with small filament

SEM Imaging



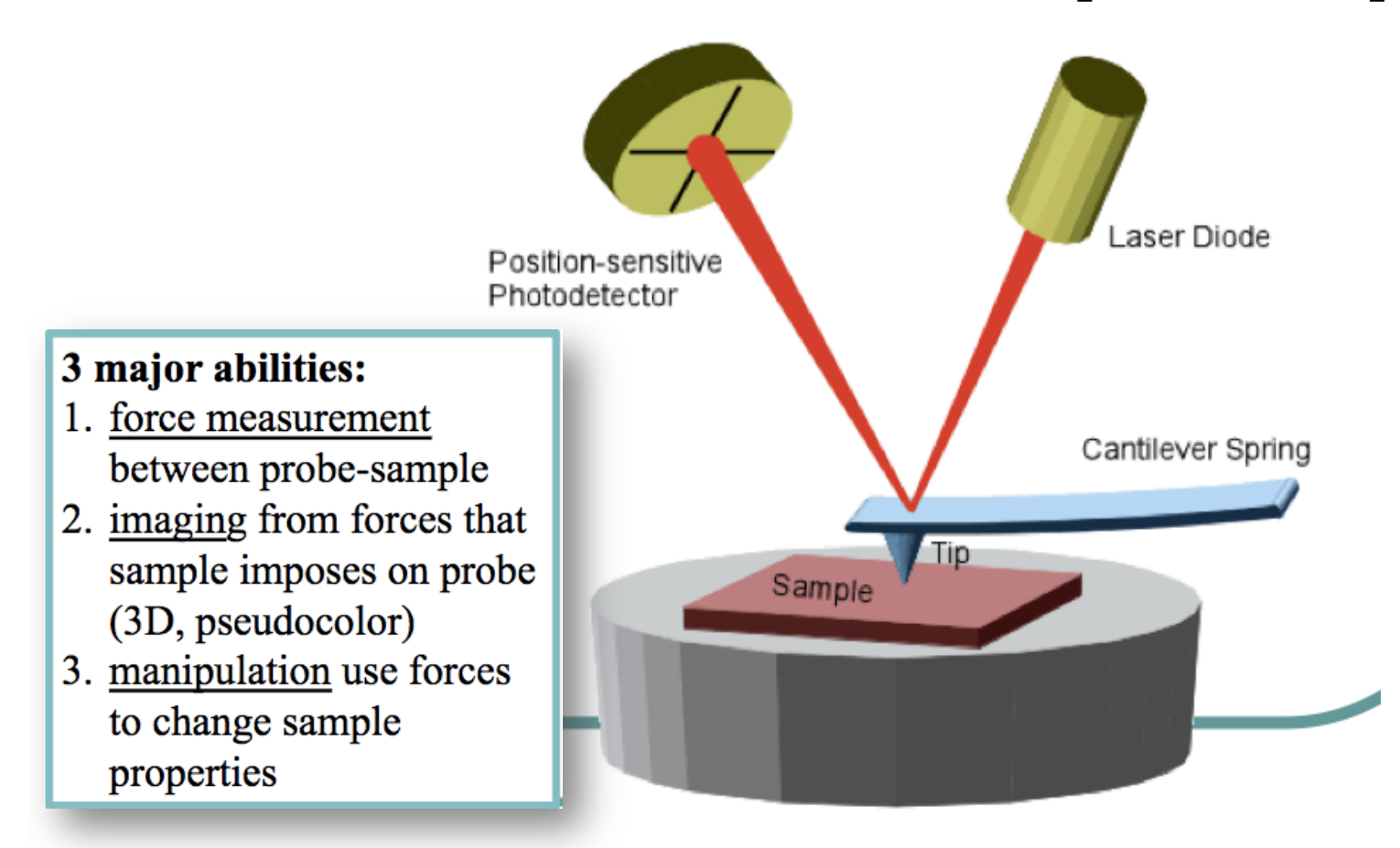
End part of Nodularia (cyanobacteria in filament shape)

SEM Imaging



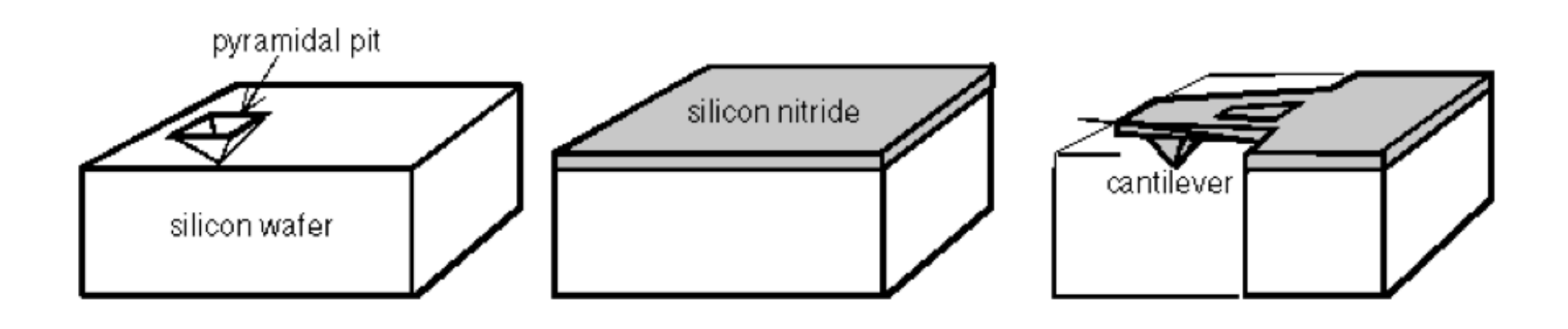
Carbon Nanotubes with a metallic nanoparticels located at the apical part

AFM detection principle



Detection principle is obtained by monitoring the bending of the cantiliver that host the tip

AFM Tip fabrication



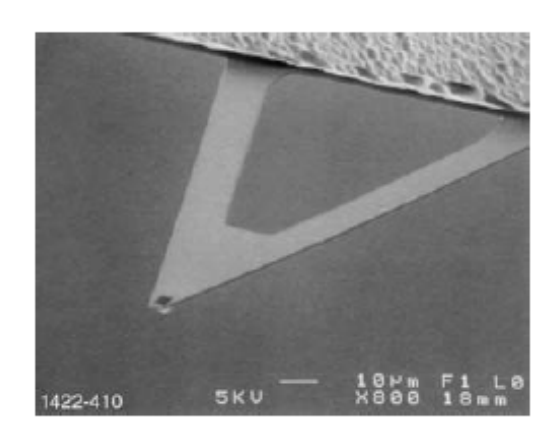
Pit etching in Si

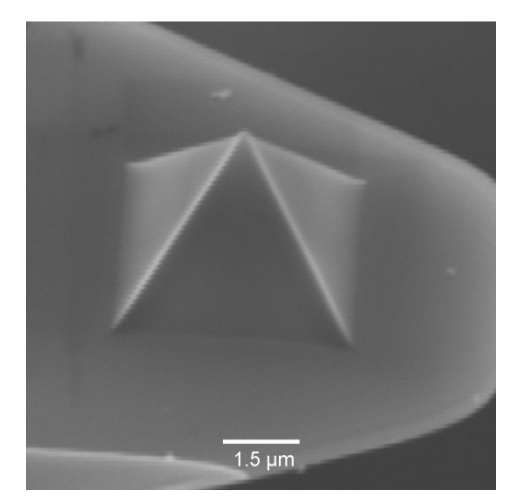
Si₃N₄ coating

Si underetching

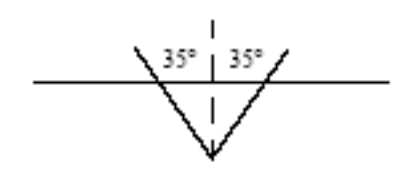
AFM tips are typically sculpted on silicon wafers

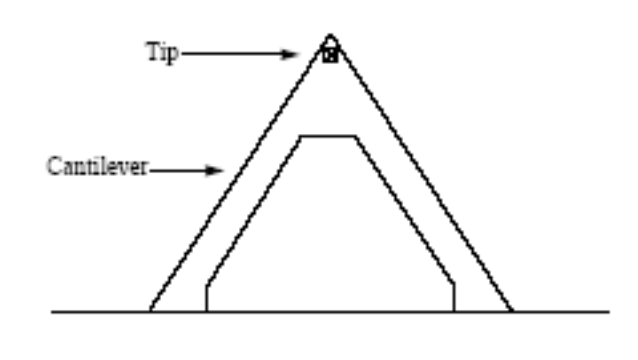
SEM on Silicon nitride probes





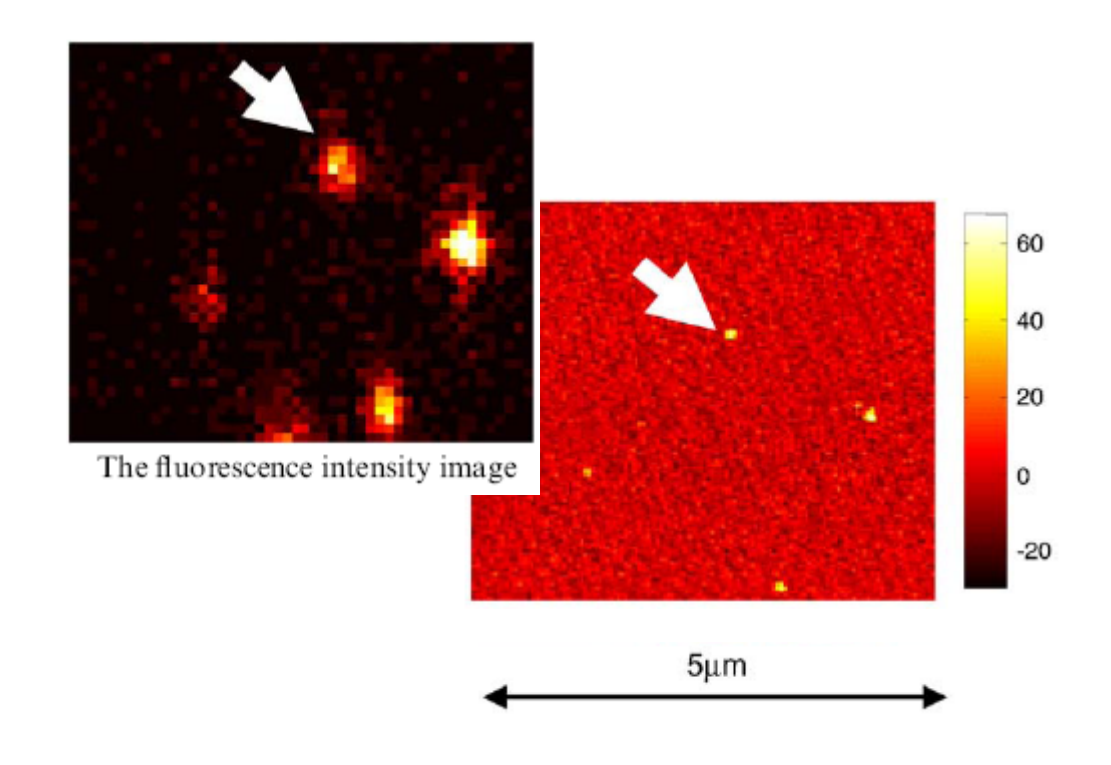
Tip Sidewall Angles of Silicon Nitride Probes





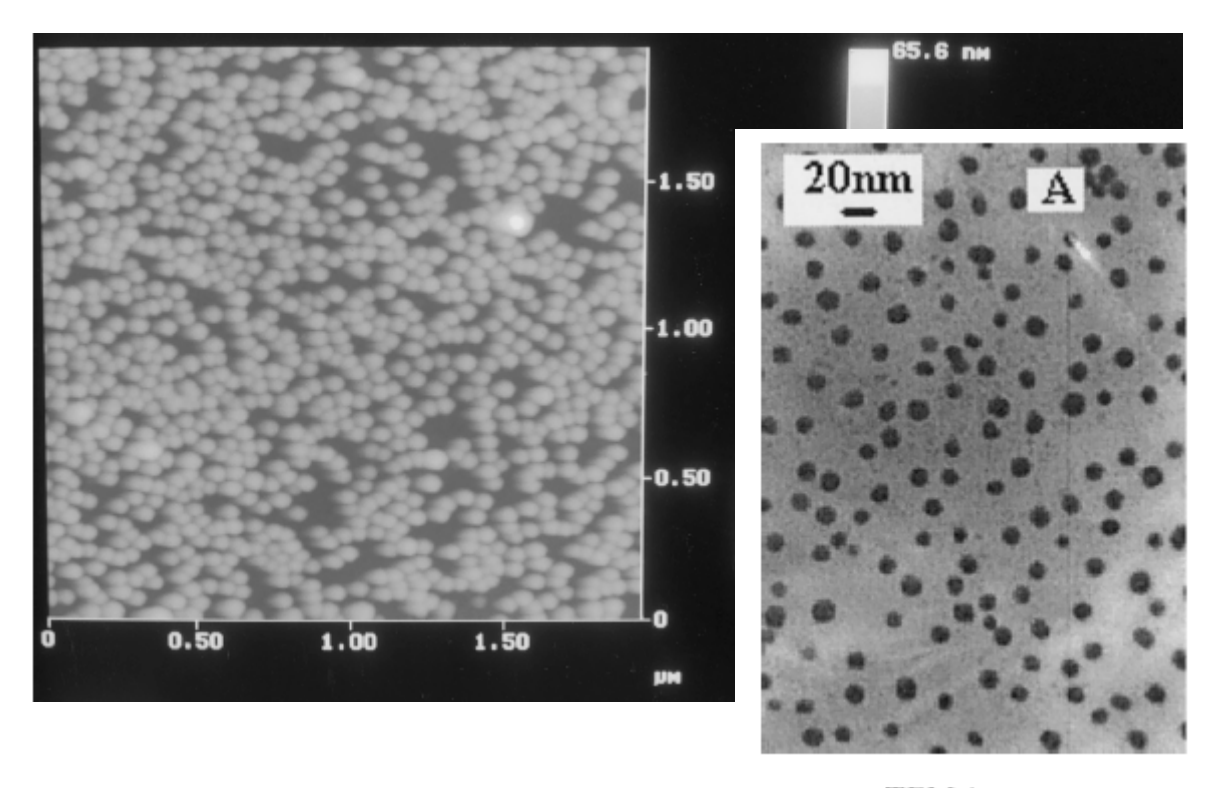


Optics versus AFM



Fluorescent Nanoparticles with average size of about 40 nm

AFM Imaging



TEM images

Gold nanoparticles made off gold core and a thiols-shell to stabilize the particle

AFM Imaging

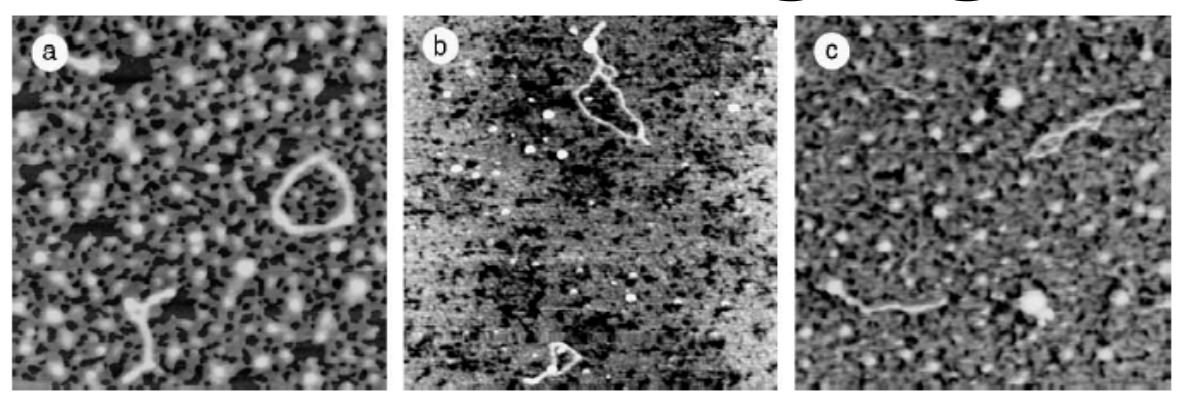


Fig. 1. Representative AFM images of plasmid DNA on the surface of newly cleaved mica at room temperature: open circular structure (a) $(2 \mu m \times 2 \mu m)$, supercoiled structure (b) $(2.5 \mu m \times 2.5 \mu m)$ and relaxed supercoil (c) $(2 \mu m \times 2 \mu m)$.

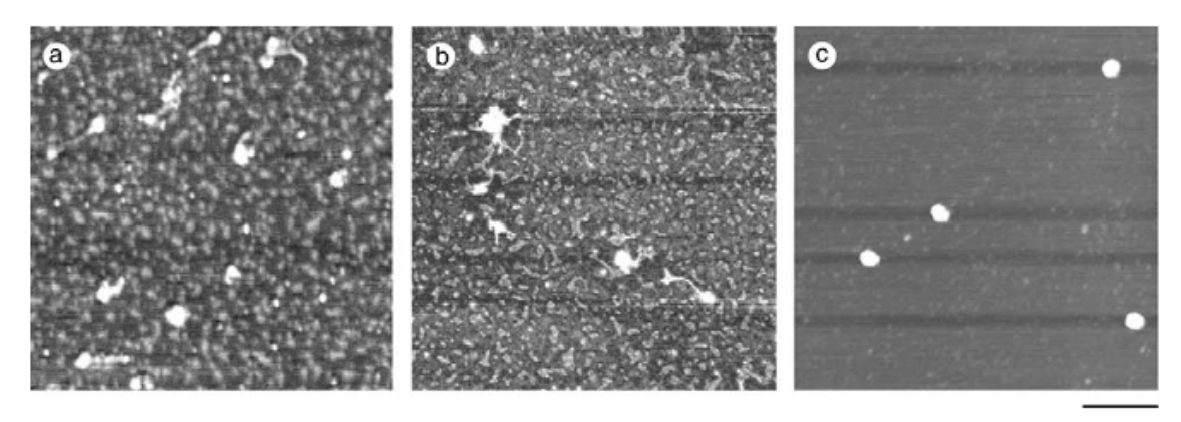
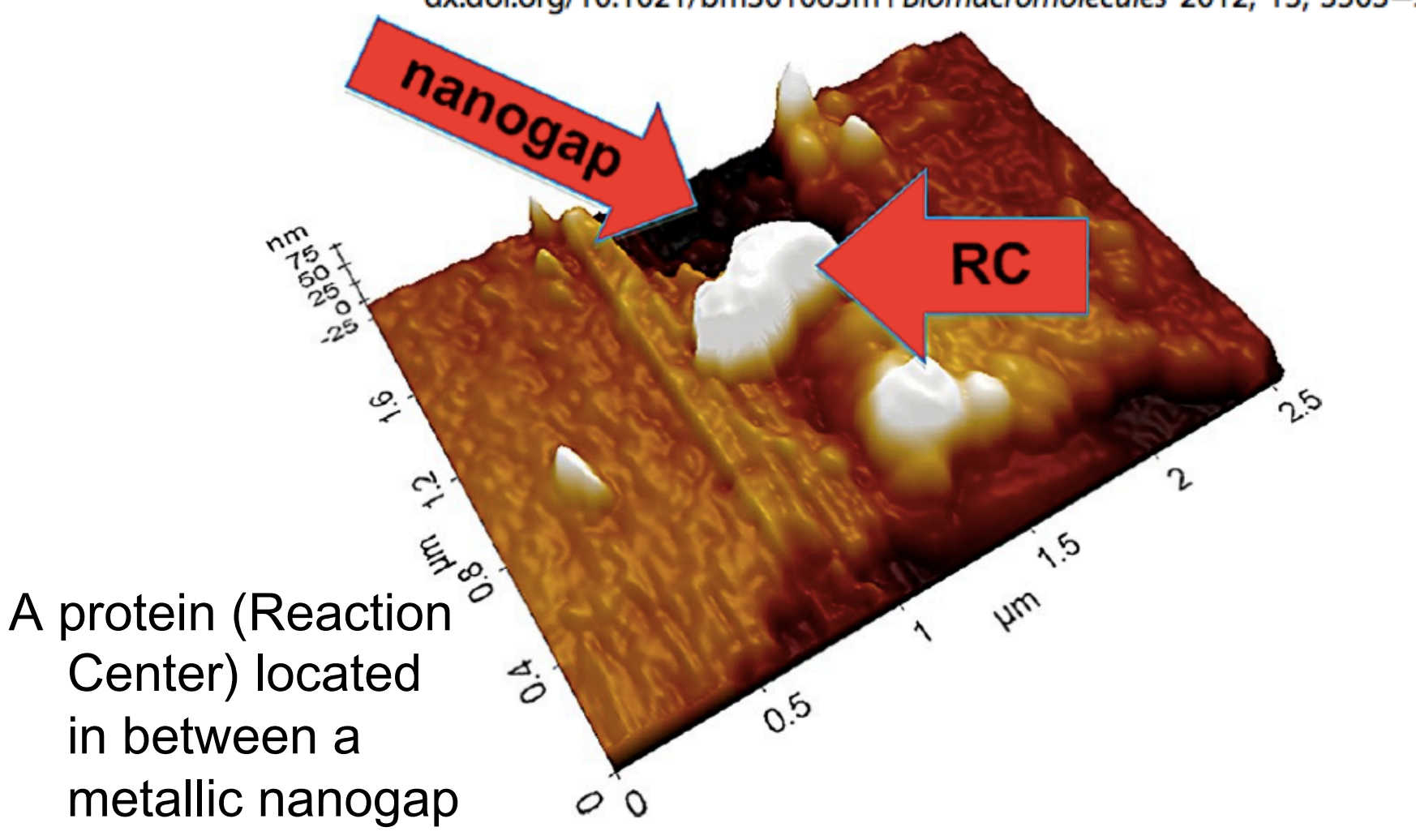


Fig. 2. Representative AFM images of plasmid DNA on the surface of mica after heated at 80 °C (a), 84 °C (b) and 90 °C (c). In both (a) and (b) circular structure disappear and formed globule structure with undenatured tail. (c) Only globule structure appear, which correspond to whole denaturation of DNA. Scale bar 500 nm for all images.

DNA

AFM Imaging

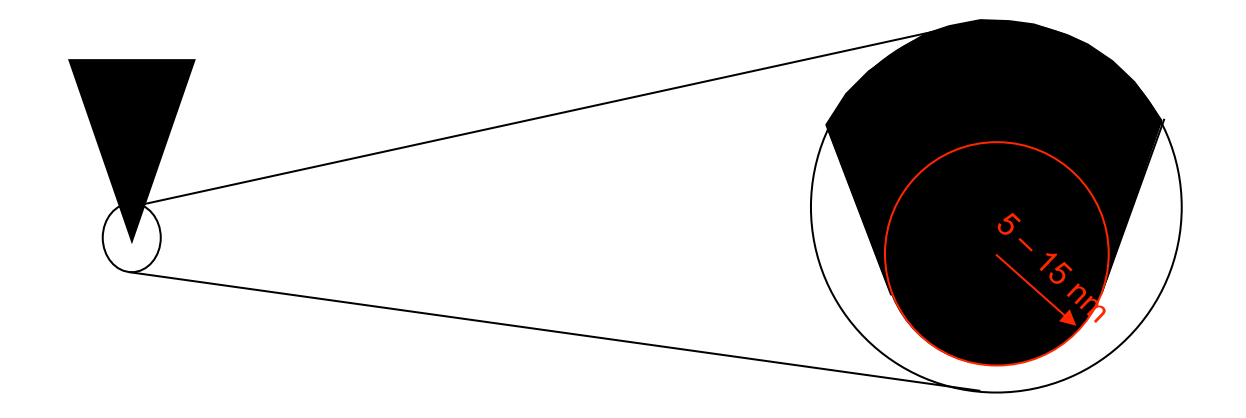
dx.doi.org/10.1021/bm301063m | Biomacromolecules 2012, 13, 3503-3509



Lateral resolution

Lateral resolution is primarily determined by the radius of curvature of the tip end.

Typical tip radii quoted by the manufacturers for tapping mode tips are around 5 – 15 nm

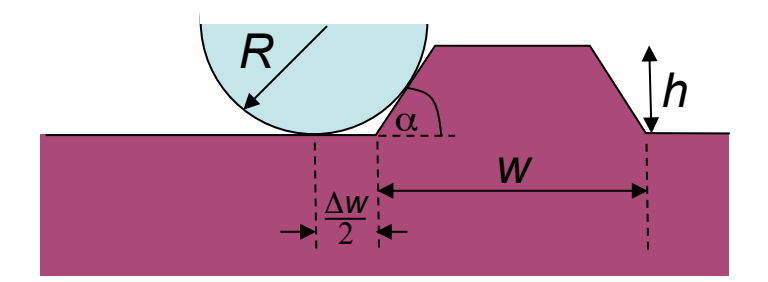


The sidewall angles of the tip will also determine its ability to probe high aspect ratio features.

Errors in width measurements

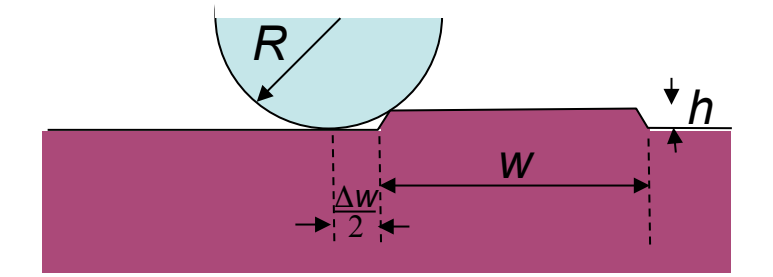
Assuming a hemispherical tip:

 $h > R(1-\cos\alpha)$



$$\frac{\Delta w}{2} = R \tan \frac{\alpha}{2}$$

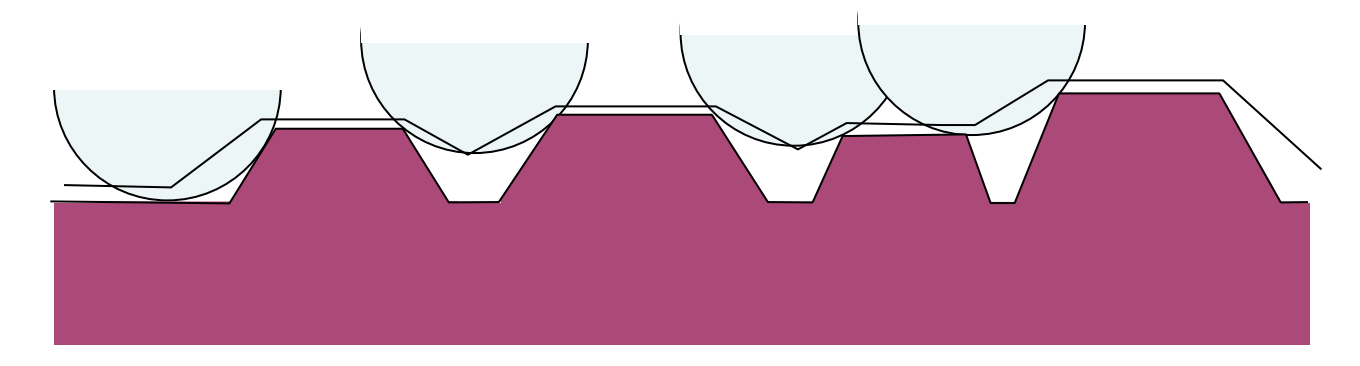
 $h < R(1-\cos\alpha)$



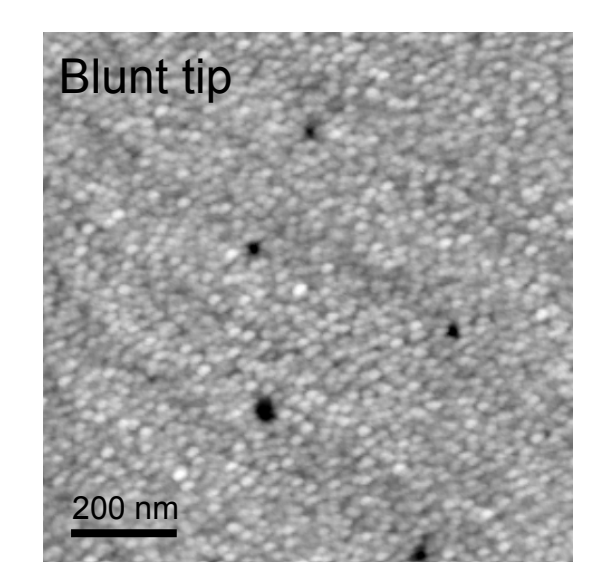
$$\frac{\Delta w}{2} = \sqrt{h(2R - h)} - h\cot\alpha$$

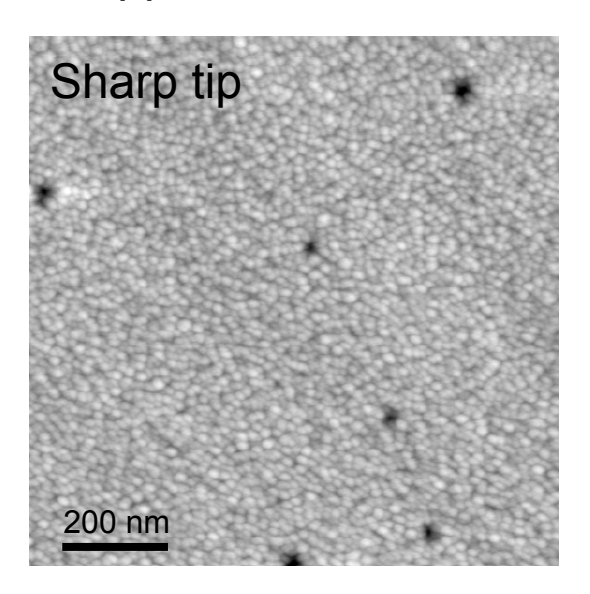
Not only the tip radius but the feature height and its likely shape must be known to accurately determine the true width

Dense nanostructure arrays

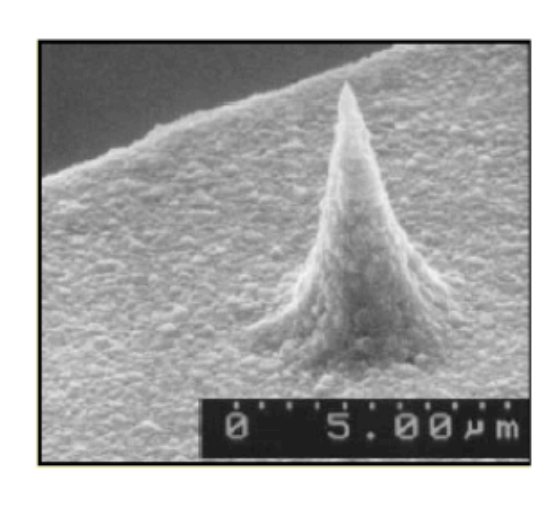


For densely packed features the tip size can also cause errors in determining the height of the islands, or the overall appearance of the surface

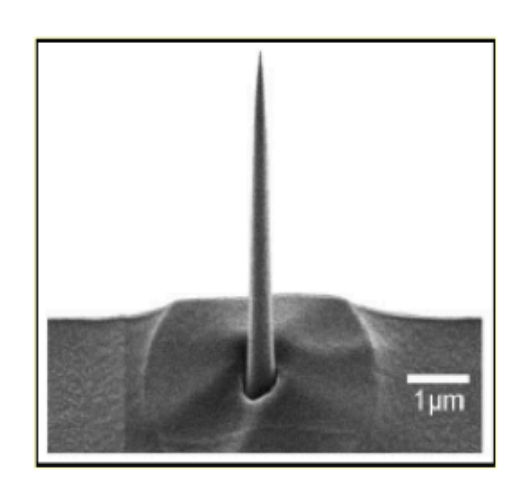




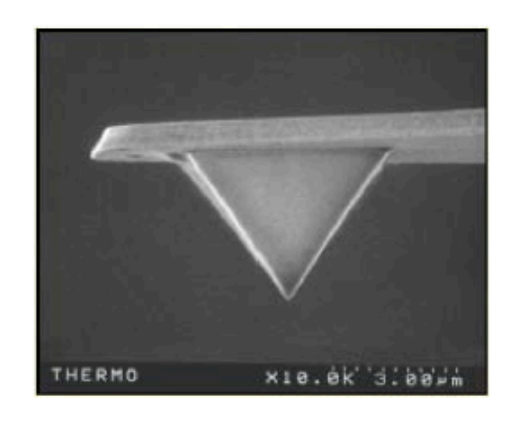
Special AFM tips



Diamond-coated tip



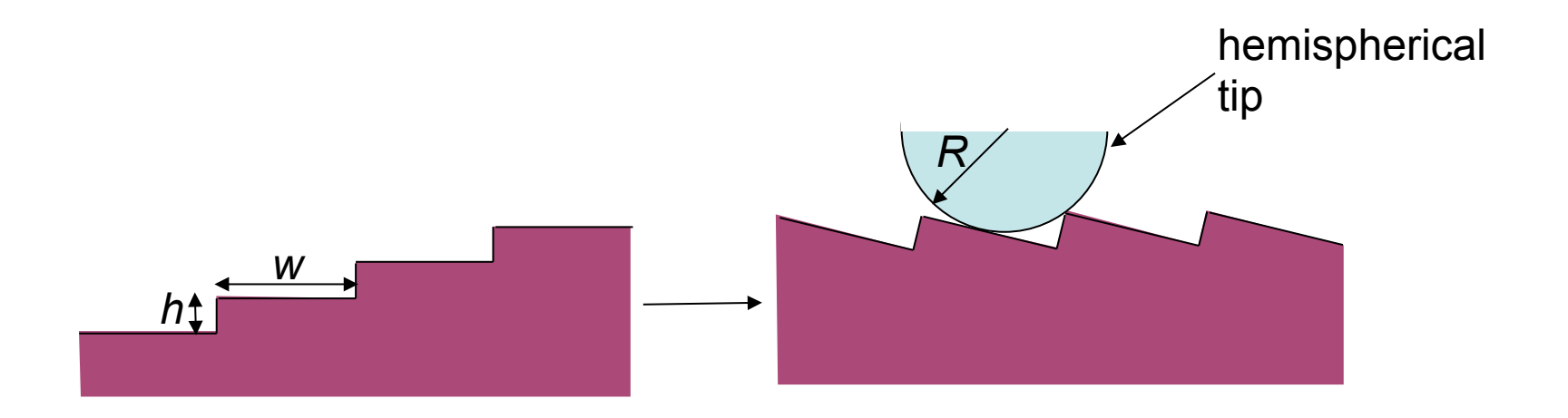
FIB-sharpened tip



Gold-coated Si₃N₄ tip

Special tips are sometimes used to further increase the miscroscope resolution

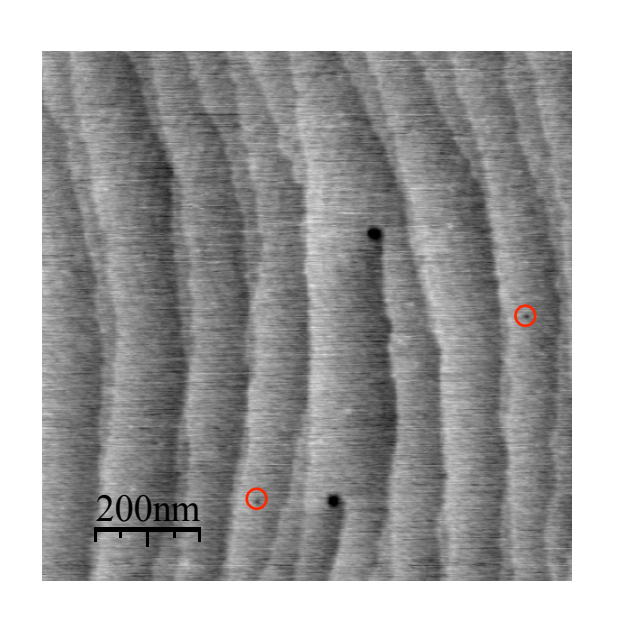
Terraced surfaces

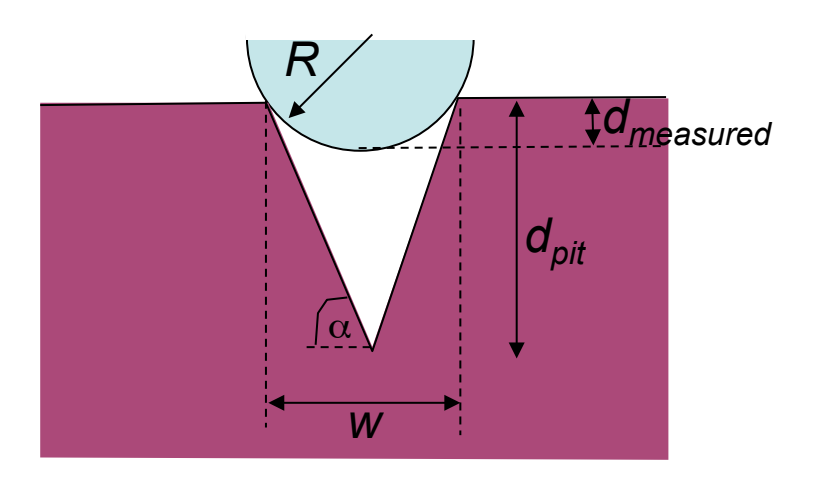


Single atom-high steps may be routinely imaged by AFM.

However, as step-edges become closer together (e.g. on vicinal substrates) it may become impossible to see separate terraces.

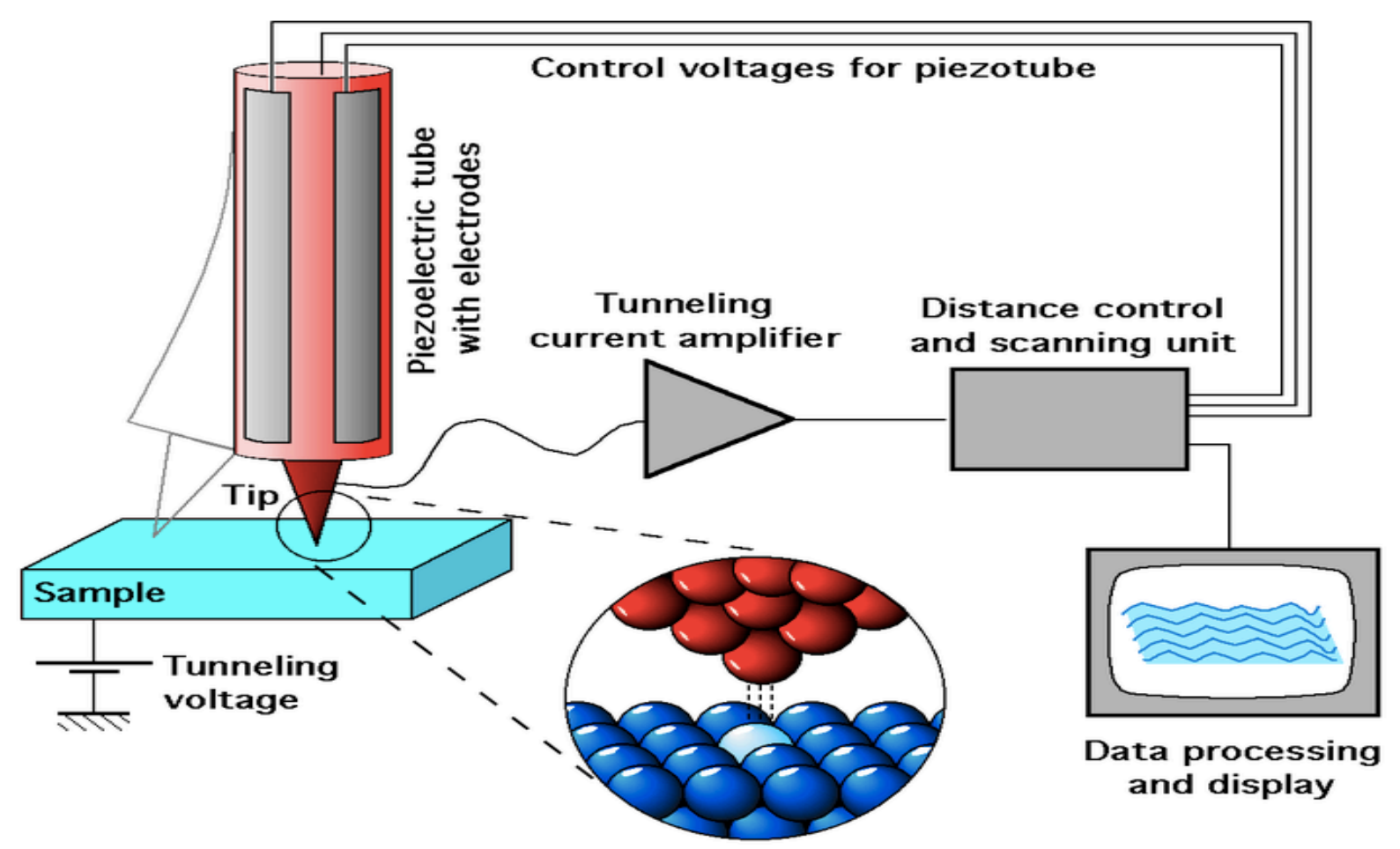
Small pits





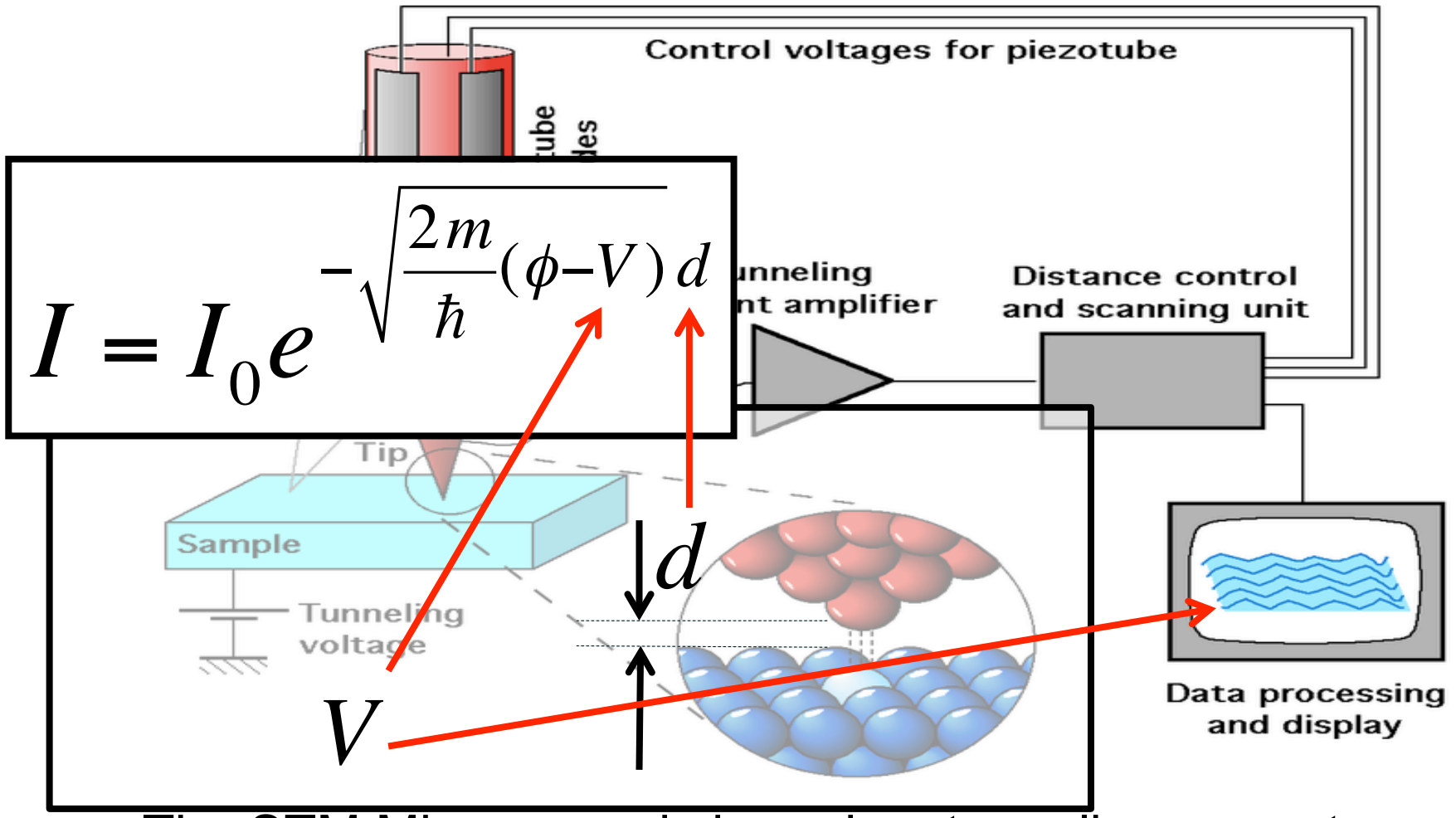
When imaging small pits, such as pits associated with threading dislocation terminations, one is unlikely to see the true pit depth. The measured width will actually by more accurate than the measured depth, which will depend on the angle α , and the tip radius. The pit will not be visible if the measured depth is less than the noise level.

STM Microscopy



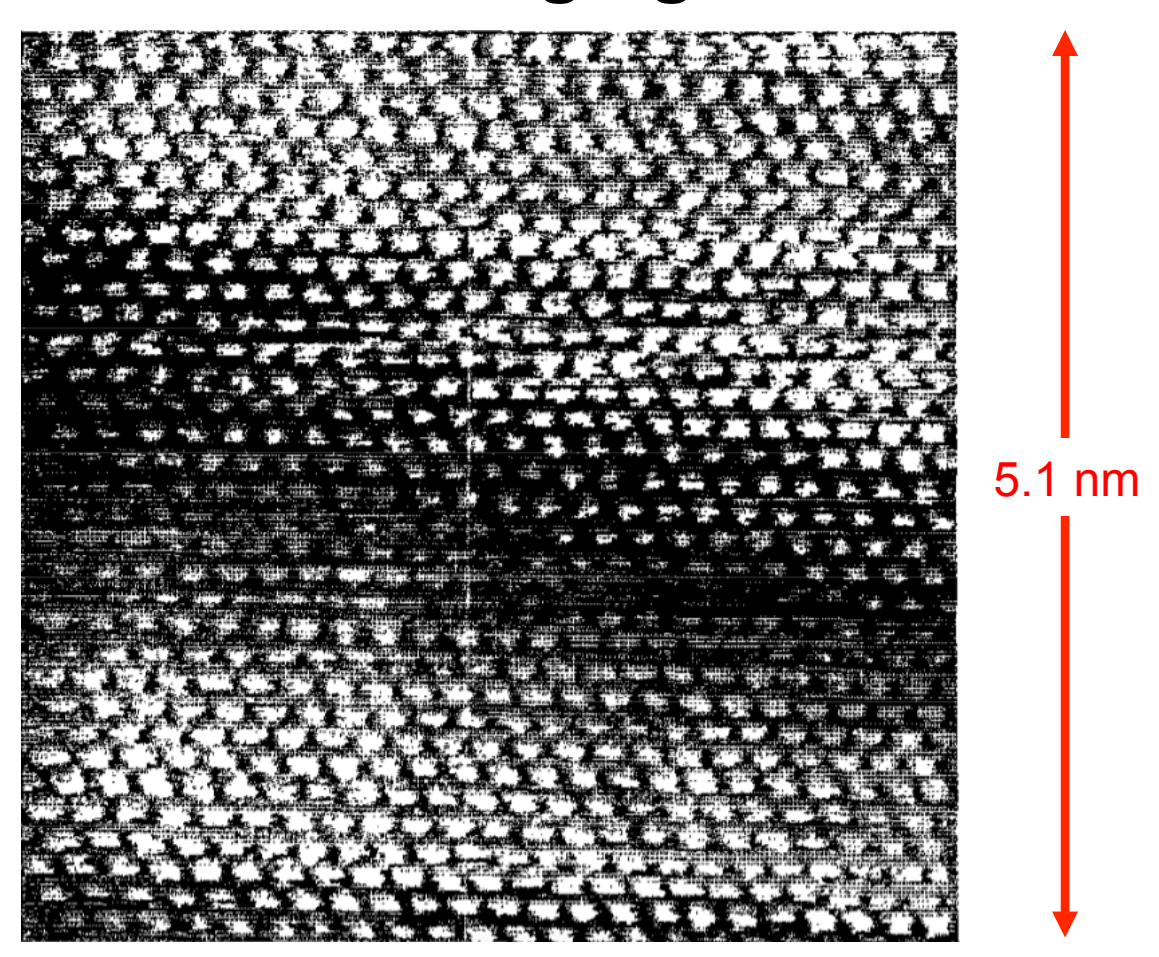
The STM Microscopy is based on tunneling currents as established in between the tip and the sample

STM Microscopy



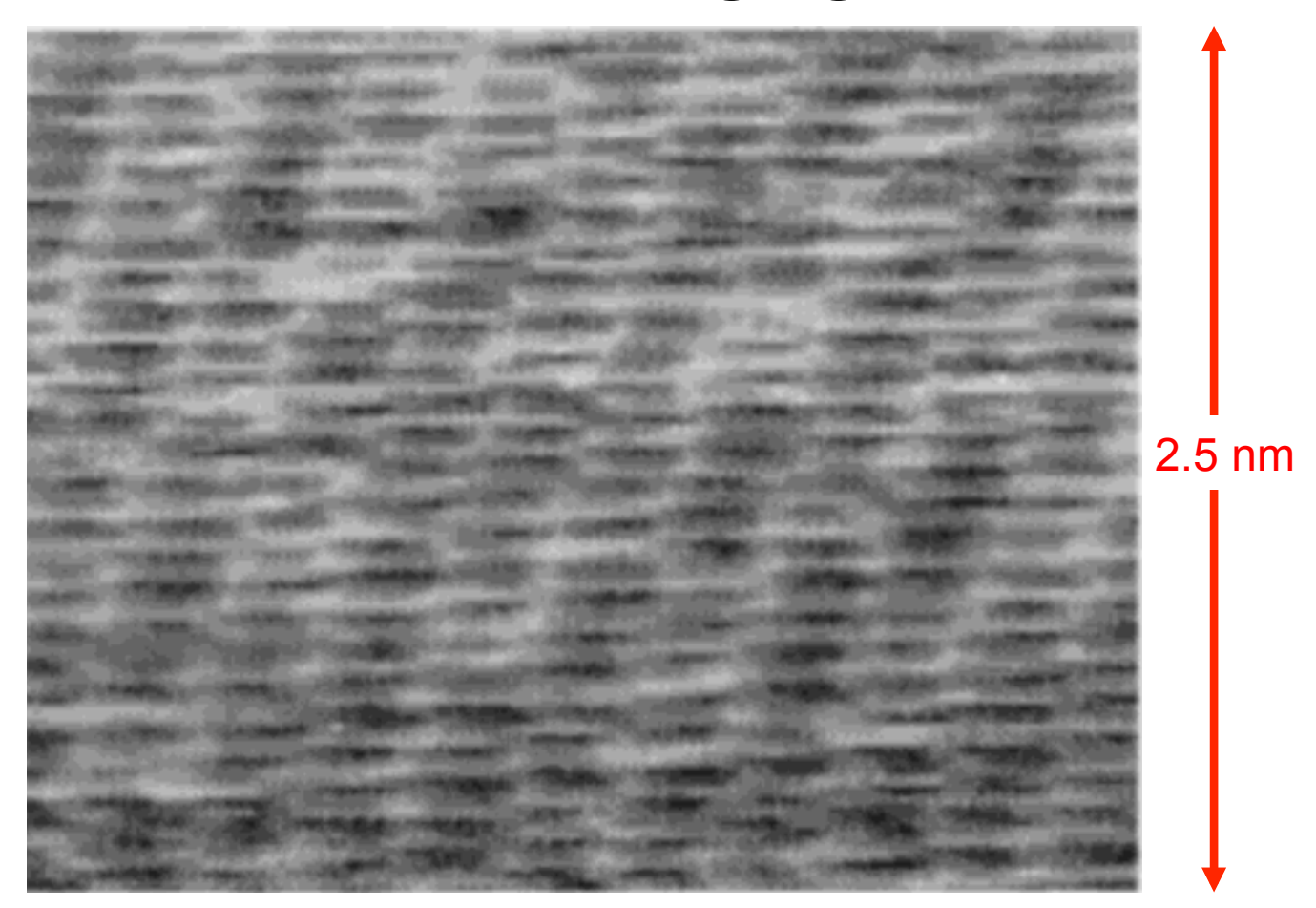
The STM Microscopy is based on tunneling currents as established in between the tip and the sample

STM imaging



Carbon atoms in the lattice structure of the highly oriented pyrolytic graphite. Image by STM in air.

STM imaging



Organic molecules (thiols) self-assembled onto highly oriented pyrolytic graphite. Image by STM in air.